

Gravity Indicators in the Near-Infrared Spectra of Brown Dwarfs

N. I. Gorlova, M. R. Meyer, G. H. Rieke, J. Liebert

Steward Observatory, The University of Arizona, 933 N. Cherry Ave., Tucson, AZ 85721

ngorlova@as.arizona.edu, mmeyer@as.arizona.edu

ABSTRACT

We investigate the sensitivity to temperature and gravity of the strong absorption features in the J- and K-band spectra of substellar objects. We compare the spectra of giants and young M dwarfs (of low gravity) to field M and L dwarfs (of high gravity) and to model spectra from the Lyon group. We find that low-resolution spectra of M4 – M9 stars and young brown dwarfs at $R \sim 350$ and $S/N > 70$ can determine the spectral type to a precision of ± 1 subtype, using the H₂O and CO bands, and can measure the surface gravity to ± 0.5 dex, using the atomic lines of K I and Na I. This result points toward the development of photometric spectral indices to separate low-mass members from foreground and background objects in young clusters and associations. We also emphasize the complexity of the interpretation of the empirical quantities (e.g., spectral types) in terms of the physical variables (e.g., temperature, opacities) in the cool atmospheres of young brown dwarfs.

Subject headings: infrared: spectra – stars: low-mass, brown dwarfs – stars: gravity

1. Introduction

One of the central problems in stellar astrophysics is the shape of the initial mass function (IMF) at the sub-stellar end. Is it terminated somewhere below the hydrogen burning limit? Is it influenced by the conditions of the ambient medium? These questions (and others) are prompted by the theoretical speculations on opacity-limited fragmentation (Bate, Bonnell, & Bromm 2002; Boss 2001) and the boundary between the structural properties of stars, brown dwarfs (BDs), and planets (e.g., Burrows et al. 2001). In addition to studies

aimed at determining the time- and space-averaged field star IMF (e.g., Reid et al. 1999; Kroupa 2001), it is interesting to compare results from young stars to the field to search for variations in the IMF. Evidence to date suggests that the stellar IMF ($> 0.08 M_{\odot}$) in young clusters is consistent with results from the field (Meyer 2000). Previous results suggest that a universal IMF may extend into the sub-stellar regime (Luhman et al. 2000; Martín et al. 2000). However, Briceño et al. (2002) find evidence for a difference in the sub-stellar IMF between the T association in the Taurus-Auriga dark cloud and the dense Trapezium cluster associated with the Orion Nebula. It is still unclear whether the IMF truncates near the minimum mass defined by opacity-limited fragmentation in the interstellar medium (Spitzer 1978).

Observational approaches to answering these questions are hampered by the fading of the low-mass objects as they age, while the nearest birth places (where they are young and bright) are a few hundred parsecs away and often highly extinguished. Thus, the use of large telescopes and infrared instrumentation is required, and even then sensitivity limitations can make determination of fundamental parameters or even cluster membership difficult. For example, a common way to determine the IMF in young clusters is by means of broad-band photometry. However, though fast, this method suffers from contamination by foreground dwarfs and background giants, which can have the same colors and apparent magnitudes as the pre-main-sequence (PMS) population at the very lowest masses.

Another way to identify young objects is to search for signs of extreme activity. The presence of accretion disks is indicated by photometric excesses (Natta & Testi 2001; Muench et al. 2001; Natta et al. 2002; Liu 2003), sometimes accompanied by line emission and veiling (Luhman et al. 1998; Gómez & Persi 2002; Zapatero Osorio et al. 2002a,b). Young objects may also exhibit photometric variability due to modulation by rotating spots (Joergens et al. 2002). Magnetic activity may be manifested in strong X-ray emission and flares (Imanishi, Tsujimoto, & Koyama 2001; Feigelson et al. 2002; Preibisch and Zinnecker 2002). Unfortunately, the biases inherent in samples defined by these signatures of activity are not well understood.

Another approach is to conduct spectroscopic follow-up of photometric candidates. Unfortunately, conventional $R \sim 1000 - 2000$ spectroscopy is very time-consuming in the infrared. An intermediate approach would be to find a set of strong features, detectable at low resolution or even by means of narrow-band photometry, that are capable of discriminating between various types of red objects in the visible (Hillenbrand et al. 2002; Clarke, Tinney, & Covey 2002). To extend this method further into the infrared, we have searched for gravity-sensitive features in J- and K-band spectra. Young brown dwarfs (and low-mass stars) should have surface gravities intermediate between dwarfs and giants. We have obtained

near-infrared spectra of confirmed members of young open clusters (low gravity) and of field objects (high gravity). We combine photometric and visible spectroscopic data from the literature with theoretical evolutionary tracks in order to estimate the luminosities, masses, and gravities of these objects. We then attempt to disentangle the effects of temperature and gravity on the infrared spectral features of these objects, using model spectra for guidance.

2. New Observations

2.1. Sample Selection

Since our goal is to identify gravity-sensitive spectral features, we selected a sample of objects with a narrow range of spectral types (SpTs), thus removing temperature so far as possible as a variable in the data. Low-mass objects initially contract at nearly constant temperature; thus, by selecting sources from young clusters with ages from ≤ 1 to > 100 Myr we can probe gravities differing by nearly two orders of magnitude in objects of similar mass! Although field M dwarfs are much older, their gravities are only slightly larger than those of the oldest open cluster objects in our sample. However, they have the advantage of being much closer, and therefore much brighter than the BDs in old clusters.

We therefore included three types of objects in our sample, of SpT M4 – M9 and of mass $\sim 0.1M_{\odot}$: 1.) Members of the star-forming regions Taurus, ρ Ophiuchi, IC 348, σ Orionis, Upper Scorpius, and TW Hydrae; 2.) one object from the Pleiades (age ~ 120 Myr (Stauffer, Schultz & Kirkpatrick 1998)); and 3.) field dwarfs (presumed to be more than 500 Myr old) selected to match the SpTs of our cluster objects, with a few additional later-type sources. We also observed three late M giants to calibrate the low gravity end of the scale. The program objects are listed in Table 1.

2.2. Data Acquisition

We observed the sample with the near-infrared spectrometer FSpec (Williams et al. 1993) on the 6.5m Monolithic Mirror Telescope. Table 2 is a log of the observations. Source acquisition and guiding were performed with a slit-viewing infrared camera. The width of the slit was 1.0 arcsec (~ 3 pixels) and we used a 75 l/mm grating. After Gaussian smoothing with $\sigma = 1$ pixel, the final resolution of the spectra was $0.0045\mu\text{m}$ (or $R \sim 300$) in J-band and $0.0065\mu\text{m}$ (or $R \sim 350$) in K-band. The useful spectral coverage was 1.16 – 1.34 and 2.10 – 2.41 μm , respectively. Each observation consisted of four frames, each at a different position along the 30'' slit. The typical exposure time was 120s per frame. The giants were observed

on a cloudy night to avoid saturation. Each target observation was preceded and followed by an identical spectrum (except for integration time) of a field G or F dwarf, selected to be within 0.3 airmasses, to allow correction for telluric absorption.

Spectral extraction used standard IRAF tasks as well as specific routines for FSpec provided by C. Engelbracht. First, the images were dark-subtracted and bad pixels were marked (using a mask created for each night by combining flat and dark frames). Then the frames were differenced, assigning unequal weights as necessary for better airglow removal. They were divided by a dome flat and rectified to correct for the geometric distortion of the spectrograph. Finally, they were median-combined (which also removed nearly all the bad pixels). We also used the data to obtain a pure airglow spectrum, which was used for wavelength calibration. After extracting an object spectrum, it was divided by a similarly reduced telluric standard spectrum and the result was multiplied by a normalized solar spectrum to correct for absorption lines in the standard. We multiplied the resultant spectrum by a blackbody spectrum of temperature corresponding to the SpT of the standard and finally smoothed the result in the IRAF task `gauss` with the `sigma` parameter set to one pixel. No absolute calibration was attempted; all the spectra were normalized to the same scale based on averages over the spectral regions 1.185 - 1.305 μ m or 2.100 - 2.340 μ m. The spectra are shown in Figures 1, 2.

3. Source Properties

3.1. Properties of PMS Sub-giants and Field Dwarf Stars

3.1.1. Surface Gravities

Although it is clear qualitatively that younger objects have lower gravity, quantitative analysis requires estimates of $\log(g)$ that rely in part on theoretical evolutionary models. Thus, to further analyze the spectral features we need to determine the surface gravities of the objects.

We estimated the gravities according to

$$\log(g) = 4.42 + \log\left(\frac{M}{M_{\odot}}\right) - \log\left(\frac{L}{L_{\odot}}\right) + 4 \times \log\left(\frac{T_{eff}}{5770}\right) \quad (1)$$

Temperatures were obtained from the spectral types, luminosities were based on bolometric corrections to dereddened I- or J-band magnitudes, and masses were determined from theoretical tracks on the $L - T_{eff}$ diagram as described below. Relevant references to the

literature are included in Table 1, and the source properties we derive are listed in Table 3. The locations of the sample objects in the H-R diagram for a subset of tracks and one temperature scale are illustrated in Figure 3.

3.1.2. Luminosities

Luminosities were calculated according to:

$$\log\left(\frac{L}{L_{\odot}}\right) = 1.86 - 0.4 \times (J - 0.265 \times A_V + BC_J + 5 - 5 \times \log(d)) \quad (2)$$

This equation assumes $M_{bol\odot} = 4.64$ ($BC_{V\odot} = -0.19$, Binney & Merrifield (1998, p.60)) and $A_J = 0.265 A_V$ (Cohen et al. (1981)), J in the CIT system.

The J band is optimal for luminosity estimation in young low-mass objects for several reasons (Meyer, Calvet & Hillenbrand 1997; Luhman 1999; Natta et al. 2002): 1.) most of our sources are not heavily reddened and at temperatures of 2000 – 3000K, so the peak of their spectral energy distributions falls within this band; and 2.) the J band is also situated in the range least contaminated by UV and IR excesses due to possible accretion disks or other forms of circumstellar material. For a few USco objects missing J magnitudes, we estimated them from I magnitudes by combining the (I – J) colors of USco objects of similar SpTs from Ardila, Martín, & Basri (2000) with the field dwarf SpT – (I – J) relationship from Dahn et al. (2002, their Fig.4), adopting (I – J) to be 2.15, 2.20, and 2.40 magnitudes for M5.5, M6, and M7 respectively. For the hottest star in our sample (G1 569A), the bolometric magnitude was derived from m_V and BC_V (assumed to be -1.49 for M1.5), since no infrared photometry is available for this star.

The extinction for cluster objects was taken from the literature, where it was usually derived by de-reddening the sources using intrinsic colors inferred from known spectral types. Since the true colors of young BDs are not yet well-established, field dwarf colors were used for reddening determination. We later justify this procedure by showing that these young objects are much closer in spectral properties to dwarfs than to giants and that the features used in the optical spectral classification (TiO, VO) are not very sensitive to gravity for temperatures higher than ~ 2500 K. For field dwarfs thought to be within 25 parsecs of the Sun, we assumed $A_V = 0.0$.

Bolometric corrections (BC_J) were calculated by averaging SpT vs. BC_J data from three sources: Wilking, Greene & Meyer (1999) for M dwarfs, Reid et al. (2001) for L dwarfs, and Dahn et al. (2002) for both M and L dwarfs.

Our distance estimates are based on the HIPPARCOS convergent-point and parallax results (Perryman et al. 1997; de Zeeuw et al. 1999) and those by Monet et al. (1992) and Dahn et al. (2002). The only exception is the Pleiades, where we adopted recent result from main sequence fitting (Stello & Nissen 2001), and incorporated the difference between two independent estimates (0.25 mag) into the distance modulus error. For 2MASSJ1139-3159, a member of the TW Hydra association, the distance is comparable with the size of association itself, and is therefore very uncertain. The distance uncertainty was included in estimating the effects of observational errors on the physical properties in Section 3.1.5. For the seven field dwarfs with unknown distances, we adopted M_J from the M_J vs. SpT relation of Dahn et al. (2002). For the only T dwarf in our sample (SDSS 1624+0029, T6), we adopted luminosity and temperature equal to those of Gl 229B (T6.5), as given in Leggett et al. (2002, Table 7), since no reliable BCs are available for T dwarfs yet.

3.1.3. Temperatures

Effective temperatures of our sources were estimated based on their SpTs. There are two difficulties in this procedure. First, the dwarf temperature scale is uncertain by $\pm 200\text{K}$ as shown in Figure 4, where we compile some recent temperature estimates from the literature. Second, the same spectral type may not correspond to the same temperature in a dwarf, a PMS object, and a giant. Due to the paucity of direct T_{eff} measurements (low-mass eclipsing binaries for linear diameter measurements are yet to be discovered), most temperature scales are based on comparison with models. However, the models may still be inadequate. For example, Lucas et al. (2001) derived SpTs of substellar sources in the Trapezium by comparing de-reddened H-band spectra to those of field dwarfs. They then used Dusty99 model spectra by Allard, Hauschildt, & Schweitzer (2000) to derive temperatures, which turned out to be very hot for their late types compared to the field, even allowing for subdwarf gravities (Figure 4). On the other hand, Natta et al. (2002) using the same but slightly updated model spectra on the low-resolution *full* JHK spectra of young BDs in ρ Oph, arrived at a dwarf temperature scale. We will comment further on this discrepancy in Section 5.1.

Taking into account these uncertainties, we based our temperature estimates on observationally based calibrations: two of them (Luhman 1999; Wilking, Greene & Meyer 1999, further WGM99) were used to study the low mass population of young clusters, and the other (Dahn et al. 2002) is based on the trigonometric parallaxes to field dwarfs. The average value of the temperature from these three calibrations for each program object is given in Table 3.

3.1.4. *Evolutionary Tracks and Masses*

There are three state-of-the-art sets of theoretical tracks available for low-mass objects, differing in the treatment of interior structures and especially atmospheres: 1.) those of Burrows et al. (1997) are well-suited for the lowest mass BDs and planetary-mass objects; 2.) D’Antona & Mazzitelli (1997, 1998) (DM97, DM98) use gray atmospheres and calculate tracks for very young objects; and 3.) the Lyon group includes constraints from detailed atmospheric codes – dust-free “NextGen” (Hauschildt, Allard & Baron 1999; Hauschildt et al. 1999) and more realistic at cooler temperatures “Dusty” (Allard et al. 2001) – to construct BCAH98 (Baraffe et al. 1998) and Dusty00 (Chabrier et al. 2000) evolutionary tracks, respectively. However, we should bear in mind that none of the current models is capable of describing adequately ages less than 1 Myr (Baraffe et al. 2002). While many of our cluster objects probably fall within this age range, the resulting systematic uncertainties in estimating their gravity (which would affect our results) seem to be < 0.5 dex as described below.

As one can see from Table 3, our program objects (except for WL 14, Gl 569A, and GJ 402) lie in the vicinity of, or below the BD boundary at $0.075 M_{\odot}$. For our study it is not necessary that all the objects be BDs, because the transition from the stellar to the substellar regime is continuous in terms of luminosity, temperature, and other properties. Table 3 shows that the average masses of young and old objects in our sample are very close, allowing us to consider the spectra as an evolutionary sequence.

We adopted the average of the gravities estimated independently from three sets of tracks and three temperature scales (Figure 5). As can be seen from Table 3 and Figure 6, the gravities of the young objects are well-separated from those of field dwarfs: $\log(g) = 3.0 - 4.2$ for the former, and $5.0 - 5.5$ for the latter. M giants have much lower gravities than dwarfs of either age range, $\log(g) = 0.0 \pm 0.5$ (Section 3.2).

3.1.5. *Uncertainties in the Physical Parameters*

There are two major types of uncertainty in the physical parameters in Table 3: 1) those systematic uncertainties due to the choice of theoretical tracks and the SpT/ T_{eff} relations; and 2) random uncertainties due to measurement error and uncertainties in calibrations. We consider each in turn.

As explained above, we averaged estimates from several sets of theoretical tracks rather than giving preference to one of them. The dispersion among these estimates provides a sense of the uncertainty due to *theory* in our results. However, there may also be systematic

errors that affect the results of all the models in similar ways, an issue that is difficult to treat quantitatively.

Thus, for each object we have assigned from one to three values of T_{eff} using SpT/ T_{eff} relations from Dahn et al. (2002); Luhman (1999); Wilking, Greene & Meyer (1999). The average values are given in Table 3 and used in Figure 6. The agreement among these temperature scales is of about 80K for field objects, and 130K for cluster objects. There is a parallel observationally based error due to the uncertainty in SpTs of ± 1 subtype for cluster objects and half of this amount for field objects. Including the effects of the dispersion in the Dahn et al. (2002) SpT/ T_{eff} relation of ± 100 K (their Figure 7), we arrive at an uncertainty in T_{eff} due to measurement error of 120K for field dwarfs and 150K for cluster members. These latter errors are used in the following discussion as they are larger than those from the indicated range of possible temperature scales. We note that Luhman (1999) finds the typical offset between dwarf and subgiant scales is +150K from M6 – M8, of order the random uncertainties adopted here.

Measurement errors also cause uncertainty in the estimated luminosities. Thus, the measurement errors in m_J (0.05 for the field, 0.1 for cluster members) and the mismatches of the various photometric systems employed (≤ 0.1 magnitudes for 2MASS, CIT, and UKIRT for cool stars (Carpenter 2001)) have been combined quadratically to obtain an estimate of $\sigma(m_J) = 0.10$ magnitudes for field stars and 0.15 for cluster members. In addition, there are errors in the extinction as a result of uncertainties in both the color measurements and the intrinsic colors. We have estimated these effects from the relations between SpT and the $I - J$ and $J - K$ colors from Dahn et al. (2002). We obtain $\sigma(A_J) = 0.3$ magnitudes (or ~ 1 mag in A_V) for cluster objects, and neglect extinction error for those in the field. In converting m_J to luminosity, we have taken an uncertainty in BC_J of 0.05 magnitudes for M dwarfs and 0.20 for L dwarfs (based on the scatter in the BC_J vs. SpT relations in Dahn et al. (2002); Reid et al. (2001); Wilking, Greene & Meyer (1999)). Finally, we have calculated errors in luminosity due to uncertainties in the distance moduli individually for each object. For the field dwarfs where we have used spectroscopic parallax to estimate the distance moduli, we estimate the error to be 0.35 magnitudes. The resulting total errors in luminosity from combining all of these effects are shown in Figure 3 and entered in Table 3. They average 0.18 dex for cluster objects and 0.11 dex for those in the field.

These errors in observational parameters cause uncertainties in the derived parameters such as mass and gravity. From mass estimates using the three temperature scales and three sets of theoretical tracks, we find a dispersion for cluster members of $0.024 M_\odot$, and of $0.012 M_\odot$ for field stars. An observational contribution to the uncertainty in mass arises because of the uncertainties in L and T_{eff} . We estimate it for each object from Fig. 3 as the range

of masses on evolutionary tracks that pass through 1σ errorbars in T_{eff} and L . We find this uncertainty to be on average about $0.025 M_{\odot}$ for cluster members and $0.019 M_{\odot}$ for field stars. Similarly, the uncertainties in $\log(g)$ due to the theoretical tracks and temperature estimates were estimated from the dispersion in results for individual stars to be 0.26 dex for cluster members and 0.10 dex in the field. Observational errors in $\log(g)$ result from errors in mass, temperature, and luminosity. Propagating the error estimates for these quantities, the $\log(g)$ errors are 0.30 dex in clusters and 0.18 dex in the field. For both mass and $\log(g)$, the observational component is larger and has been entered in Table 3.

To summarize, sources of random error appear to be as large or larger than the sources of systematic error considered here. In all cases, we have adopted the “observational” random errors in our quantitative analysis.

3.2. Properties of Giants

3.2.1. Masses and Gravities

For giants, we estimated $\log(g)$ from the literature, based on luminosity class and spectral type: $\log(g) = 0.5 \pm 0.5$ for M1 – M8 III stars (Tsuji 1986; Houdashelt et al. 2000). The assumed masses of these stars lie between 1 and $5 M_{\odot}$. The dominant source of uncertainty is variability in SpT and magnitude. Full infrared light curves are generally unavailable for long-period variables. Based on those reported by Lockwood & Wing (1971), Nadzhip et al. (2001), and Bedding et al. (2002), we estimate typical variations for our stars to be less than 1 magnitude. No infrared photometry is available for BD+14 2020, so we estimated its m_J from m_V and the $V - J$ colors taken from Ducati et al. (2001) and Perrin et al. (1998).

Fortunately, the properties of the giants are sufficiently well removed from dwarfs (particularly for gravity) that rough estimates suffice for our purposes.

3.2.2. Temperatures

For SpTs between M0 and M7, the giant temperature scales in the literature agree to within $\pm 100\text{K}$, but by M8 the differences increase to 200K (Perrin et al. 1998; van Belle et al. 1999; Hauschildt et al. 1999). We used the median of the range of quoted SpTs for the giants to determine T_{eff} and BC_J from Table 4 of Hauschildt et al. (1999). Taking the uncertainty in the temperature calibrations to be $\sim 100\text{K}$, and an uncertainty in SpT of ± 2 subtypes, we derive an overall uncertainty in T_{eff} of 320K .

4. Analysis of Near-Infrared Spectral Indices

Armed with estimates of the temperature and gravity for all objects in our sample, along with associated uncertainties, we can now investigate the correlations of near-infrared spectral features with physical properties.

In Figure 7 we show candidate spectral indices for temperature and gravity: FeH ($1.20\mu\text{m}$), K I ($1.25\mu\text{m}$), H₂O ($1.34\mu\text{m}$), Na I ($2.21\mu\text{m}$), Ca I ($2.26\mu\text{m}$), and CO ($2.30\mu\text{m}$). The indices are defined in Table 4. They have been selected to measure features that are prominent at low spectral resolution (Joyce et al. 1998; Luhman et al. 1998; McLean et al. 2000; Wallace et al. 2000). The width for H₂O and CO ($2.30\mu\text{m}$) bands can be extended depending on the local telluric water vapor content and the desired S/N. In Table 5, we report equivalent widths for the absorption lines due to FeH, K I, Na I, and Ca I as well as flux ratios for H₂O and CO.

First we assess the measurement uncertainties in indices, then the model spectra used for reference, and finally analyze the observed dependence of spectral features on temperature and gravity.

4.1. Uncertainties in Indices

The most straightforward method to estimate uncertainty in the strength of an index would be to compare the index strength on a few independent spectra of a given object. However, due to the reduction process that we adopted (the spectrum was extracted from a combined 2-dimensional frame, *not* by combining separately extracted 1-dimensional spectra), we could not realize this method for all our objects. Instead, we derived a simple analytic expression that relates an easily measured S/N in flux (ideally on the featureless part of the combined spectrum) to the desired uncertainty in the index strength:

$$\sigma_{index} = \frac{A_{index}}{S/N_{cont}} \quad (3)$$

Here, A_{index} represents six empirical coefficients corresponding to our six indices. These coefficients were treated as constants and were calibrated by inverting Equation (3) for two of our objects adopted as “error standards” - 2MASS1707 (field dwarf) and USco67 (cluster member). σ_{index} in the “error standards” was calculated by comparing index values measured in spectra extracted from individual, non-combined frames, and by dividing the mean square deviation of these values by the square root of the number of frames – as described at the beginning of this section.

We computed S/N_{cont} for each object as a mean square deviation in flux over the regions 1.2890 - 1.3080 μm (J band) and 2.2230 - 2.2822 μm (K band). In these late-type stars, it is impossible to find a spectral region free of lines. Hence, S/N_{cont} is only meaningful in a relative sense, as an estimate of the quality of the object spectrum relative to that of the “standards”. It is a lower limit on the real S/N in the continuum for giants, where the repeatability of features (Figure 2) indicates the presence of many real lines in these wavelength regions. Then we used expression (3) to calculate the errors in the index strength for a given star (Table 5).

The uncertainty associated with the correction for telluric features is not accounted in this approach. To assess this effect, one would need to obtain several spectra of an object at different times, airmasses, and reduced with different telluric standards. Since we were unable to carry out such an extensive study, we are unable to tell whether the observed scatter in spectral indices at a given SpT and $\log(g)$ is due to other relevant physical parameters, or to observational errors.

4.2. Theoretical Spectra

Figure 6 shows the domains of the synthetic spectra calculated by the PHOENIX code of the Lyon group.¹ We used the BD Dusty and BD Cond 2000 models (Allard et al. 2001) to compare to our observations. These models represent two extreme cases for the treatment of dust. The first assumes a uniform distribution of interstellar-sized particles over the whole atmosphere, with a high level of thermal emission by the dust. The second assumes that the only important effect of the dust is to remove the refractory elements from the gas (the condensation, or rain-out model). Emission by dust effectively reduces the equivalent widths of the absorption spectral features, and it is thought to be relevant in M6 – L8 dwarfs, while the Cond models should be applicable to later spectral types. However, we only find significant differences in the near infrared between Cond and Dusty model spectra for T_{eff} below 2300K (Figures 7, 9), which corresponds to \sim L0, while most of the objects in our sample are of SpT M6 – M8. The hotter stars are in the dust-free regime where both models produce identical results.

NextGen models do not consider dust formation and in addition use outdated H₂O and TiO opacities. However, they are the most recent PHOENIX models available for giant gravities, so we use them in the comparison with the data on giants.

¹The model calculations can be found at <http://phoenix.physast.uga.edu>

4.3. Sensitivity to Temperature and Gravity

Figure 8, a plot of SpT vs. index strength, is a traditional way of assigning spectral types. If we concentrate on *field* objects only (circles), we see that most features follow a smooth sequence, corresponding to change in temperature. For example, the EW of K I peaks at L2.5, Na I at M6, Ca I earlier than M3, and FeH at L2.5. The broad H₂O and CO bands increase monotonically in strength to saturation in the mid-Ls. These results are in good agreement with the higher-resolution near-infrared studies by Ali et al. (1995), Luhman et al. (1998), McLean et al. (2000), and Reid et al. (2001), among others. They are also consistent with optical studies of FeH (e.g. Kirkpatrick et al. 1999; Martín et al. 1999). The temperatures of peak intensity for alkali-metal lines correlate with their first ionization potentials. The decline at lower temperatures is due to grain formation and complex molecular chemistry rather than excitation considerations.

However, including *cluster* objects and *giants* (crosses and triangles) introduces both systematic effects and increased scatter. To explore the possibility that gravity is responsible for the scatter, we plotted the indices vs. gravity in Figure 9. We grouped our objects according to SpT (bearing in mind that the uncertainty in SpTs is ~ 1 subtype) and denoted each group by a unique symbol. We also over-plotted measurements from the theoretical spectra, choosing temperatures representative of our SpT groups. We discuss the results by specific index.

4.3.1. K I & Na I

K I and Na I lines in the optical and near-infrared are known to be systematically weaker in cluster BDs compared to the same SpT in the field (e.g., Martín, Rebolo & Zapatero Osorio 1996; Luhman et al. 1998; Béjar, Zapatero Osorio & Rebolo 1999; Lucas et al. 2001; Martín et al. 2001; Gizis 2002). However, no systematic study of the gravity-dependence is available, particularly of the 1.25 μm feature of K I, which is conveniently situated near the middle of the J band.

As indicated both by the models and our observations, for a given T_{eff} (or SpT), the K I line becomes systematically weaker at low gravities. To increase the statistical significance, we have fitted this behavior after first combining the data for M6 – M8 subtypes. We used a linear least-squares routine that takes both the errors of $\log(g)$ and EW into account (Press et al. 1992). We obtained the following relation (working range M6 – M8, $3.0 > \log(g) > 5.5$):

$$\log(g) = 2.12(\pm 0.27) + 0.40(\pm 0.05) \times EW(KI_{1.25}, A) \quad (4)$$

Substituting into this expression average values of EW for the cluster and field dwarfs ($3.45 \pm 0.5 \text{ \AA}$, $\log(g) = 3.5$ and $7.71 \pm 0.5 \text{ \AA}$, $\log(g) = 5.2$, respectively) and quadratically propagating the errors, we find that the uncertainty in the spectroscopically determined $\log(g)$ from Equation 4 is 0.38 dex and 0.51 dex respectively for our low- and high-gravity objects. The uncertainties are larger than the uncertainty of the "physical" $\log(g)$ obtained from the evolutionary tracks for our objects (≤ 0.3 dex, see Section 3.1.5). This difference is a natural outcome of the fact that the temperature dependence of these indices cannot be neglected especially for high gravity objects (see Figures 8, 9). The Na I line at $2.2 \mu\text{m}$ shows a similar trend with $\log(g)$ (Figure 9) but the effect is weaker. Better modeling of this line is needed as well (Figure 7).

With more objects, one could construct a more reliable EW – $\log(g)$ – SpT relation, especially from intermediate-age clusters (like α Per) where one could probe the gravity range 4.5 – 5.0 dex.

4.3.2. FeH

As with the atomic lines just discussed, this molecular feature is both temperature and gravity sensitive, growing in strength with lower temperatures until the early Ls, and also with higher gravities. Although this trend is clear, it is difficult to derive a quantitative relation from our observations, or from models. Observationally, the EWs are uncertain, especially in cluster objects (where the feature is weak), because the feature is situated at wavelengths where our S/N is low. Current models fail to reproduce correctly the strong FeH band in early L dwarfs (see also McLean et al. (2000); Leggett et al. (2001). For example, the Cond and Dusty model predictions are very different for this feature at 1800K as shown in Figure 9. There are two reasons for these problems: 1.) the feature is very broad and may be contaminated by unidentified lines; and 2.) the transition from M to L types is marked by the onset of dust formation, which strongly modifies the pseudo-continuum formed by the adjacent water band. Thus, FeH has potential as a gravity indicator, but additional observational and theoretical work is needed to establish its behavior.

4.3.3. CO

The simple interpretation is that gravity is responsible for the difference between the strong $2.3\mu\text{m}$ CO band in K – M giants and the weaker one in dwarfs (Kleinmann & Hall 1986). This argument suggests that the strength should be intermediate in young BDs. The smaller ratio of $\text{EW}(\text{Na I} + \text{K I})/\text{EW}(\text{CO})$ measured in low-mass cluster members (Greene & Meyer 1995; Greene & Lada 1997; Luhman et al. 2000) compared to the field seems to support this idea. However, in the absence of reliable SpTs, it is difficult to tell whether the effect was due to weakening of Na I and Ca I, or to strengthening of CO with lower gravity in late-type stars. Thus, Martín et al. (2001) had to invoke veiling from a circumstellar disk when they found that CO was actually weaker in the Taurus BDs compared to a field dwarf.

Except for USco85, for which the continuum in our measurements clearly looks problematic at the red edge (Figure 2), the CO band does not look much different between cluster and field objects, in agreement with the results of Luhman et al. (1998) on IC 348 and Greene & Meyer (1995) on ρ Oph. Interestingly, the models predict CO to weaken slightly up to $\log(g) \leq 3.8$, without the need to invoke veiling in very cool objects. The models predict CO absorption deeper (smaller index values in Figure 9) than that observed, but the agreement in behavior is reasonable for the Cond models. Thus, the previously assumed monotonic behavior of CO with gravity does not hold over the range of spectral types considered here. The CO lines form a nice monotonic sequence over SpTs M5 – L2 for dwarfs, and since they seem to be only slightly gravity-dependent, they can be used for reliable temperature estimation in young low mass objects.

4.3.4. H₂O

The H₂O bands are the strongest features in the near-infrared spectra of late M to early L dwarfs and therefore have been widely used for spectral classification at low resolution (e.g. Testi et al. 2001). Detailed comparisons of models and data by Jones et al. (1995) showed that the water bands are much more sensitive to temperature than gravity and metallicity. Nevertheless, gravity effects have been reported in the literature. Yet, as with CO, the size of these effects remains to be explored. Lucas et al. (2001) claim that for an optically classified young M dwarf one would expect water absorption in the H band to be as strong as in field L dwarfs. However, Wilking et al. (2003) find no significant difference in the water absorption strength in the K band between M dwarfs and sub-giants.

Our measurements of the water index show a good correlation with SpT. After CO, it has the least scatter compared with the rest of the indices. There is, however, an indication

that on average, the feature may be stronger in the young objects (Figure 9). To estimate this trend quantitatively, we carried our linear fits separately for the low and high gravity groups (the numbering convention for SpTs is following: M5 = -5, L0 = 0) :

$$\begin{aligned}
 SpT &= 10.99(\pm 6.06) - 17.45(\pm 7.68) \times (F_{1.34}/F_{1.32}), \log(g) < 4.5 \\
 SpT &= 21.23(\pm 7.82) - 29.11(\pm 9.56) \times (F_{1.34}/F_{1.32}), \log(g) > 4.5
 \end{aligned}
 \tag{5}$$

Since our sample is biased against late-type cluster dwarfs (they are too faint), we are limited to the SpT range M5.5 – M8.5 only. The coefficients of the fits differ by $\sim 1.5 \sigma$. Thus, use of this index may lead to a slight overestimation of a young BD SpT in comparison with field dwarfs. However, the effect is within the uncertainty of the input SpTs of our sample, ± 1 subtype. Therefore, we confirm the result by Wilking et al. (2003) that, at least within the M spectral types, the water bands can be safely used (with 1 subtype precision) for the estimation of SpT in low-mass objects, independent of gravity (age).

The models confirm this observational conclusion by showing a very weak dependence on $\log(g)$, which in addition is not monotonic. The strengthening of H₂O absorption at low gravities, which might have been observed in H band by Lucas et al. (2001), is predicted only for temperatures $\leq 2000\text{K}$, characteristic of L dwarfs. However, even allowing for the uncertainty in the temperature of $\pm 150\text{K}$, Cond models clearly over-predict the strength of this water band. Dusty models work better, but only for the high-gravity L dwarfs (Figure 9).

4.3.5. *Ca I*

The Ca I line is strongly temperature sensitive. Unfortunately, it disappears around M7, making its measurement uncertain in our objects except for the earliest ones. The gravity sensitivity of this feature remains to be investigated.

4.3.6. *Giants*

M giants are most easily recognizable by their very deep CO bands, comparable to the ones in L dwarfs, but they lack the strong water absorption of the latter objects. The H₂O absorption is at least as weak as that in M dwarfs, confirming the recent result of Wilking et al. (2003). Na I and Ca I lines are very prominent, which is the opposite of what one would expect if they monotonically decreased with gravity. To summarize, giant spectra are very

different from their sub-giant and dwarf star counterparts. However, they do not define an extreme endpoint of a monotonic sequence in observable surface gravity effects in the J- and K-band spectra over the range of spectral types considered here (M1 – M8).

5. Discussion

Through our comparison of observed J- and K-band spectra as a function of surface gravity, and with synthetic spectra from the Lyon group, we have seen that: 1) CO and H₂O are suitable temperature indicators for young M dwarfs; and 2) K I and FeH can provide rough estimates of log(g) given an estimate for the temperature range of the target star. Are there any systematic errors that we have neglected in our analysis that could mimic the results we have obtained by observing the young, late-type objects in our sample? We describe two possible sources of systematic error, discuss why we think they do not affect our results, and demonstrate how our analysis can be used to confirm membership for candidate members of young associations.

5.1. Optical Indices and Spectral Classification of Young BDs

Perhaps the adopted spectral types (obtained from visible wavelength spectra) for PMS stars in our sample are systematically in error as a function of surface gravity. We need to determine the gravity-dependence of the indices used for spectral classification in the *optical* (Table 1) to ensure that the existing SpT classification, which is based on comparison to field dwarfs, can be applied to BDs with sub-giant gravities. To investigate this, we measured indices defined in Kirkpatrick et al. (1999) in BDcond00 model spectra (smoothed to the 9 Å resolution used by Kirkpatrick et al. (1999)) and plotted the contours of equal index strength on the log(g) – T_{eff} plane. A few characteristic patterns are shown in Figure 10. It is satisfying to see that “color” indices and the oxide molecules (TiO, VO, H₂O, CO) that are most frequently used for spectral classification of M stars, are relatively gravity-independent.

However, this behavior holds only over a limited range of parameter space. For example, for the spectral classification of sources with log(g) ranging from 3 to 5 dex, one would like to use indices behaving similarly to the “color-b” index for M5 – M9 objects (~ 2300 – 3000K) and to use “TiO-a” for M5 – M7 (~ 2700 – 3000K). After estimating the SpT, one could then use atomic lines (Na I, K I) and possible hydride molecular bands (FeH, CrH, CaH) to infer gravity (and hence young cluster membership) for the objects of interest. More general lessons are 1) to be aware of strong gravity dependence where $\frac{\partial index}{\partial T_{eff}} = 0$ (Fig. 10)

and 2) always assign spectral type based on a few different indices – in order to avoid biases associated with the individual gravity dependence of a single index.

However, we prefer calibration of object indices on standard stars, rather than directly to models. Models can provide the correct qualitative behavior, but not necessarily a good quantitative match. For example, if one tries to use the water band at $1.3 - 1.6\mu\text{m}$ and PHOENIX spectra, even with the proper gravity one will overestimate the temperature because the synthetic band is obviously too deep for a given T_{eff} (our Figures 7, 9; see also Leggett et al. (2001, Fig.9); and Natta et al. (2002, their Fig.3)). This effect is our explanation for the very hot temperatures derived by Lucas et al. (2001) for young sources in Orion.

Uncertainties in current spectral synthesis models include: 1) incompleteness of the opacity lists (Burrows et al. 2002; Cushing et al. 2002); 2) the treatment of dust (Allard et al. 2001; Tsuji 2002); 3) the dependence on initial conditions for young objects (Baraffe et al. 2002), as well as other effects. Because of these limitations, we did not try to derive our own temperature scale by comparing J and K spectra with synthetic spectra. Some of the dangers are exposed by apparent inconsistencies; for example, from Figure 9, one would conclude that M6 corresponds to $T_{eff} > 3000\text{K}$ looking at the Na I, H₂O, and CO features, while according to K I and FeH, M6 corresponds roughly to 2500K.

5.2. Other Effects at Young Ages

Perhaps our spectra are affected by activity associated with youth that could mimic the observed effects we attribute to surface gravity. One could argue that effects such as continuum veiling from accreting material could make lines weaker in cluster objects. For example, Jayawardhana, Mohanty & Basri (2002) have discovered a broad, asymmetric H α line in GY5, indicative of on-going accretion. Martín et al. (2001) report emission in Br γ in CFHT-BD-Tau4, as well as strong H α . These observations extend into the BD range the well-known tendency for activity associated with youth observed in low mass PMS stars. Such accretion activity tends to be accompanied by continuum excess emission in the near-infrared that can dilute photospheric features (Hartigan, Edwards, & Ghandour 1995).

According to our data, both GY5 and CFHT-BD-Tau4, members of the 0.3–1 Myr old embedded ρ Oph and 1–3 Myr Taurus-Auriga T association respectively, have weaker Na I and CO absorptions compared to the similar SpT USco100. USco100, an M7 member of the 5 Myr old Upper Sco subgroup of the Sco Cen OB association, has normal, single-peaked, H α emission, characteristic of coronal rather than disk accretion origin (Jayawardhana, Mohanty

& Basri 2002), but so does GY5 according to Muzerolle et al. (2003). So it is more plausible that the difference in absorption line strength that we are detecting is due to the expected age difference, reflected in lower $\log(g)$ for GY5 and CFHT-BD-Tau4. The evidence against veiling as an explanation is four-fold. First, little veiling is expected for the very low mass stars given the low mass accretion rates from their disks, as discussed by Muzerolle et al. (2003). Second, veiling should affect both molecular and atomic lines, while it is only Na I and K I, shown here to be strongly gravity-dependent, that show significant differences between cluster members and field objects. Third, neither GY5 nor CFHT-BD-Tau4 show significant evidence for continuum excess in their broad-band colors. Finally, even if moderate veiling is influencing the index strengths in the K band, it should be much less important in the J band (Meyer, Calvet & Hillenbrand 1997, Fig.2). It is unlikely that veiling is responsible for the factors of 2 – 3 difference in the line strengths between cluster and field dwarfs seen in the J band. In any case, both veiling and gravity work in the same direction, to decrease the line strengths in young objects. Therefore, weak atomic lines can be used for reliable identification of members in young clusters, regardless of the mechanism by which they are weakened.

5.3. Examples

A particularly valuable application of the gravity-sensitive indices is to identify members of nearby associations, which are typically spread over large areas on the sky and hence are seriously contaminated by interlopers. We illustrate this technique with two examples. 2MASS1139-3159 was identified as an M8 member of the young TW Hya association, based on the strength of VO and the weakness of CaH and Na I in the optical (Gizis 2002). The weakness of the FeH and K I lines in our J-band spectrum, and of the Na I line in the K spectrum compared to the field M8 dwarf 2MASS1444+3002 confirms the low gravity of this object (see Figures 1, 2). The same effect is observed in our spectra of one of the Taurus-Auriga association members, CFHT-BD-Tau4 (M7). Its membership was established by the weak K I and Na I lines in the optical and K bands (Martín et al. 2001), and we confirm this behavior in the K and J bands. As demonstrated above, spectrophotometry with SNR ~ 50 –100 derived from narrow-band filters of $R \sim 50$ –100, can be quite useful in estimating temperatures for very cool stars and distinguishing both foreground and background stars from bona fide cluster members. Additional work is needed to define a set of optimum filters at the lowest possible spectral resolution to enable efficient discrimination at modest sensitivity.

6. Summary

By inter-comparison of low resolution ($R \sim 300 - 350$) J- and K-band spectra of field and young cluster M dwarfs and M giants, and with guidance from recent model atmosphere calculations, we have arrived at the following conclusions regarding the temperature and gravity sensitivity of a number of strong near-infrared spectral features:

- The H_2O and CO bands at 1.35 and $2.30\mu\text{m}$ are relatively insensitive to gravity in the spectral range of M dwarfs, and therefore can be used for spectral classification on young stellar objects (with ~ 1 subtype precision).
- Alkali-metal lines of K I and Na I at 1.25 and $2.21\mu\text{m}$ (and possible FeH at $1.20\mu\text{m}$) can be used to derive $\log(g)$ with an uncertainty of ± 0.5 dex from $R \sim 350$, $S/N \geq 70$ spectra of M4 – M9, $3.0 > \log(g) > 5.5$ objects, given that the spectral type is known to ± 1 subtype.
- The spectra of late M giants are very distinctive from those of substellar objects. These differences can be explained in terms of their extremely low surface gravities, hotter temperature scale, and non-equilibrium processes in their tenuous atmospheres.
- The current models are unable to reproduce accurately all the observed features in these stars, and therefore should be used with caution for determination of physical parameters from spectra, especially from a single line or limited set of lines.

We would like to thank Marcia Rieke, Erick Young and John Stansberry for help with observations; Chad Engelbracht, Valentin Ivanov, Amaya Moro-Martin and Kevin Luhman for help with data reduction; and Adam Burrows and France Allard for useful discussions. NG was supported by the scholarship from the Jesuits of the Vatican Observatory; MM acknowledges support from Lucas Grant.

REFERENCES

- Ali, B., Carr, J. S., Depoy, D. L., Frogel, J. A., & Sellgren, K. 1995, *AJ*, 110, 2415
- Allard, F., Hauschildt, P. H., & Schweitzer A. 2000, *ApJ*, 539, 366
- Allard, F., Hauschildt, P. H., Alexander, D. R., Tamanai, A., & Schweitzer, A. 2001, *ApJ*, 556, 357

- Ardila, D., Martín, E., & Basri, G. 2000, *AJ*, 120, 479
- Baraffe, I., Chabrier, G., Allard, F., & Hauschildt, P. H. 1998, *A&A*, 337, 403 (BCAH98)
- Baraffe, I., Chabrier, G., Allard, F., & Hauschildt, P. H. 2002, *A&A*, 382, 563
- Barsony, M., Kenyon, S. J., Lada, E. A., & Teuben, P. J. 1997, *ApJS*, 112, 109
- Basri, G., Mohanty, S., Allard, F., Hauschildt, P. H., Delfosse, X., Martín, E. L., Forveille, T., & Goldman, B. 2000, *ApJ*, 538, 363 (Basri00)
- Bate, M. R., Bonnell, I. A., & Bromm, V. 2002, *MNRAS*, 332, L65
- Bedding, T. R., Zijlstra, A. A., Jones, A., Marang, F., Matsuura, M., Retter, A., Whitelock, P. A., & Yamamura, I. 2002, *MNRAS*, 337, 79
- Béjar, V. J. S., Zapatero Osorio, M. R., & Rebolo, R. 1999, *ApJ*, 521, 671
- Béjar, V. J. S., et al. 2001, *ApJ*, 556, 830
- Binney, J., & Merrifield, M. 1998, *Galactic Astronomy* (Princeton, NJ: Princeton University Press)
- Boss, A. P. 2001, *ApJ*, 551, L167
- Bouy, H., Brander, W., Martín, E., Delfosse, X., Allard, F., & Basri, G. 2003, *AJ*, submitted
- Briceño, C., Hartmann, L., Stauffer, J., & Martín, E. 1998, *AJ*, 115, 2074 (Briceño98)
- Briceño, C., Luhman, K. L., Hartmann, L., Stauffer, J. R., & Kirkpatrick, J. D. 2002 *ApJ*, 580, 317
- Burrows, A., et al. 1997, *ApJ*, 491, 856 (Burrows97)
- Burrows, A., Hubbard, W. B., Lunine, J. I., & Liebert, J. 2001, *Rev. Mod. Phys.*, 73, 719
- Burrows, A., Ram, R. S., Bernath, P., Sharp, C. M., Milsom J. A. 2002, *ApJ*, 577, 986
- Carpenter, J. M. 2001, *AJ*, 121, 2851
- Chabrier, G., Baraffe, I., Allard, F., & Hauschildt, P. 2000, *ApJ*, 542, 464 (Dusty00)
- Clarke, F. J., Tinney, C. G., & Covey, K. R. 2002, *MNRAS*, 332, 361
- Cohen, J. G., Persson, S. E., Elias, J. H., & Frogel, J. A. 1981, *ApJ*, 249, 481

- Cushing, M. C., Rayner, J. T., Davis, S. P., & Vacca, W. D. 2002, *ApJ*, 582, 1066
- Cushing, M. C., Tokunaga, A. T., & Kobayashi, N. 2000, *AJ*, 119, 3019
- Dahn, C. C., et al. 2002, *AJ*, 124, 1170 (Dahn02)
- D’Antona, F., & Mazzitelli, I. 1997 , in *Cool stars in Clusters and Associations*, eds. G. Micela, & R. Pallavicini (*Mem. Soc. Astron. Italiana*), 68, 807 (DM97)
- D’Antona, F., & Mazzitelli, I. 1998 , in *ASP Conf. Ser. 134, Brown Dwarfs and Extrasolar Planets*, eds. R. Rebolo, E. Martin, & M.R. Zapatero Osorio (Brigham Young University; Provo, UT), 442, 518 (DM98)
- de Zeeuw, P. T., Hoogerwerf, R., de Bruijne, J. H. J., Brown, A. G. A., & Blaauw, A. 1999, *AJ*, 117, 354
- Dieckvoss W., & Heckmann O. 1975, *AGK3 Catalog (VizieR On-line Data Catalog I/61B/agk3)*
- Ducati, J. R., Bevilacqua, C. M., Rembold, S. B., and Ribeiro, D. 2001, *ApJ*, 558, 309
- Ducati, J. R. 2002, *Catalogue of Stellar Photometry in Johnson’s 11-color system (VizieR On-line Data Catalog II/237)*
- Feigelson, E. D., Broos, P., Gaffney, J. A., III, Garmire, G., Hillenbrand, L., A., Pravdo, S. H., Townsley, L., & Tsuboi, Y. 2002, *ApJ*, 574, 258
- Freed, M., Close, L. M., & Siegler, N. 2003, *ApJ*, 584, 453
- Geballe, T. R., et al. 2002, *ApJ*, 564, 466
- Gizis, J. E., Monet, D. G., Reid, I. N., Kirkpatrick, J. D., Liebert, J., & Williams, R. J. 2000, *AJ*, 120, 1085
- Gizis, J. E. 2002, *ApJ*, 575, 484
- Gizis, J. E., Reid, I. N., & Hawley, S. L. 2002, *AJ*, 123, 3356
- Gliese, W., & Jahreiss, H. 1991, *Third Catalog of Nearby Stars (VizieR On-line Data Catalog V/70A)*
- Gómez, M., & Persi, P. 2002, *A&A*, 389, 494
- Greene, T. P., & Lada, C. J. 1997, *AJ*, 114, 2157

- Greene, T. P., & Meyer, M. R. 1995, *ApJ*, 450, 233
- Hartigan, P., Edwards, S., & Ghandour, L. 1995, *ApJ*, 452, 736
- Hauschildt, P. H., Allard, F., & Baron, E. 1999, *ApJ*, 512, 377
- Hauschildt, P. H., Allard, F., Ferguson, J., Baron, E., & Alexander, D. R. 1999, *ApJ*, 525, 871
- Hawley, S. L., Gizis, J. E., & Reid, I. N. 1996, *AJ*, 112, 2799
- Hillenbrand, L. A., Foster, J. B., Persson, S. E. & Matthews, K. 2002, *PASP*, 114, 708
- Houdashelt, M. L., Bell, R. A., Sweigart, A. V., & Wing, R. F. 2000, *AJ*, 119, 1424
- Imanishi, K., Tsujimoto, M., & Koyama, K. 2001, *ApJ*, 563, 361
- Jaschek C., Conde H., & de Sierra, A.C. 1964, *Catalog of Stellar Spectra Classified in the Morgan-Keenan System (VizieR On-line Data Catalog III/18B)*
- Jayawardhana, R., Mohanty, S. & Basri, G. 2002, *ApJ*, 578, L141
- Joergens, V., Fernández, M., Neuhäuser, R., & Guenther, E. 2002, *A&A*, submitted (astro-ph/0206137)
- Jones, H. R. A., Longmore, A. J., Allard, F., Hauschildt, P. H., Miller, S., & Tennyson, J. 1995, *MNRAS*, 277, 767
- Joyce, R. R., Hinkle, K. H., Wallace, L., Dulick, M., & Lambert, D. L. 1998, *AJ*, 116, 2520
- Kenyon, S. J., Dobrzycka, D., & Hartmann, L. 1994, *AJ*, 108, 1872
- Kerschbaum, F., & Hron, J. 1994, *A&AS*, 106, 397
- Kholopov, P. N., et al. 1998, *Combined General Catalog of Variable Stars (GCVS, VizieR On-line Data Catalog II/214A)*
- Kirkpatrick, J. D., et al. 1999, *ApJ*, 519, 802
- Kirkpatrick, J. D., et al. 2000, *AJ*, 120, 447 (Kirkpatrick00)
- Kleinmann, S. G., & Hall, D. N. B. 1986, *ApJS*, 62, 501
- Kroupa, P. 2001, *MNRAS*, 322, 231

- Lane, B. F., Zapatero Osorio, M. R., Britton, M. C., Martn, E. L., & Kulkarni, S. R. 2001, *ApJ*, 560, 390
- Leggett, S. K. 1992, *ApJS*, 82, 351
- Leggett, S. K., Allard, F., Geballe, T. R., Hauschildt, P. H., & Schweitzer, A. 2001, *ApJ*, 548, 908 (Leggett01)
- Leggett, S. K., et al. 2002, *ApJ*, 564, 452 (Leggett02)
- Liu, M. C. 2003, in *IAU Symp. 211, Brown Dwarfs*, ed. E. L. Martin (ASP), in press (astro-ph/0207477)
- Lockwood, G. W., & Wing, R. F. 1971 *ApJ*, 169, 63
- Lucas, P. W., Roche, P. F., Allard, France, & Hauschildt, P. H. 2001, *MNRAS*, 326, 695 (Lucas01)
- Luhman, K. L. 1999, *ApJ*, 525, 466 (Luhman99)
- Luhman, K. L., Liebert, James, & Rieke, G. H. 1997, *ApJ*, 489, L165
- Luhman, K. L., & Rieke, G. H. 1999, *ApJ*, 525, 440
- Luhman, K. L., Rieke, G. H., Lada, C. J., & Lada, E. A. 1998, *ApJ*, 508, 347
- Luhman, K. L., Rieke, G. H., Young, E. T., Cotera, A. S., Chen, H., Rieke, M. J., Schneider, G., & Thompson, R. I. 2000, *ApJ*, 540, 1016
- Makarov, V. V., & Fabricius, C. 2001, *A&A*, 368, 866
- Martín, E. L. & Ardila, D. R. 2001, *AJ*, 121, 2758
- Martín, E. L., Brandner, W., Bouvier, J., Luhman, K. L., Stauffer, J., Basri, G., Zapatero Osorio, M. R., & Barrado y Navascués, D. 2000, *ApJ*, 543, 299
- Martín, E. L., Delfosse, X., Basri, G., Goldman, B., Forveille, T., & Zapatero Osorio, M. R. 1999, *AJ*, 118, 2466
- Martín, E. L., Dougados, C., Magnier, E., Ménard, F., Magazzú, A., Cuillandre, J.-C., & Delfosse, X. 2001, *ApJ*, 561, L195
- Martín, E. L., Rebolo, R., & Zapatero Osorio, M. R. 1996, *ApJ*, 469, 706
- McLean, I. S. et al. 2000, *ApJ*, 533, L45

- Meyer, M. R., Calvet, N., & Hillenbrand, L. A. 1997, *AJ*, 114, 288
- Meyer, M. R., Adams, F. C., Hillenbrand, L. A., Carpenter, J. M., & Larson, R. B. 2000, in *Protostars and Planets IV*, ed. V. Mannings, A. P. Boss, S. S. Russell (Tucson: University of Arizona Press), 121
- Monet, D. G., Dahn, C. C., Vrba, F. J., Harris, H. C., Pier, J. R., Luginbuhl, C. B., & Ables, H. D. 1992, *AJ*, 103, 638
- Montes, D., Martín, E. L., Fernandez-Figueroa, M. J., Cornide, M., & de Castro, E. 1997, *A&AS*, 123, 473
- Muench, A. A., Alves, J., Lada, C. J., & Lada, E. A. 2001, *ApJ*, 558, L51
- Muzerolle, J., Hillenbrand, L., Calvet, N., Briceño, C., & Hartmann, L. 2003, *ApJ*, in press (astro-ph/0304078)
- Nadzhip, A. E., Tatarnikov, A. M., Shenavrin, V. I., Weigelt, G., & Yudin, B. F. 2001, *Astronomy Letters*, 27, 324
- Natta, A., & Testi, L. 2001, *A&A*, 376, L22
- Natta, A., Testi, L., Comerón, F., Oliva, E., D'Antona, F., Baffa, C., Comoretto, G., & Gennari, S. 2002, *A&A*, 393, 597
- Preibisch, T., & Zinnecker, H. 2002, *AJ*, 123, 1613
- Perrin, G., Coude Du Foresto, V., Ridgway, S. T., Mariotti, J.-M., Traub, W. A., Carleton, N. P., & Lacasse, M. G. 1998, *A&A*, 331, 619
- Perryman, M. A. C., et al. 1997, *A&A*, 323, L49 (The Hipparcos Catalog)
- Press, W. H., Teukolsky, S. A., Vetterling, V. T., & Flannery, B. P. 1988-1992, *Numerical Recipes in Fortran* (Cambridge: Cambridge University Press)
- Reid, I. N., et al. 1999, *ApJ*, 521, 613
- Reid, I. N., Burgasser, A. J., Cruz, K. L., Kirkpatrick, J. D., & Gizis, J. E. 2001, *AJ*, 121, 1710
- Reid, M. J., & Goldston, J. E. 2002, *ApJ*, 568, 931
- Schweitzer, A., Gizis, J. E., Hauschildt, P. H., Allard, F., Howard, E. M., & Kirkpatrick, J. D. 2002, *ApJ*, 566, 435 (Schweitzer02)

- Schweitzer, A., Gizis, J. E., Hauschildt, P. H., Allard, F., & Reid, I. N. 2001, *ApJ*, 555, 368
(Schweitzer01)
- Spitzer, L. 1978, *Physical Processes in the Interstellar Medium* (John Wiley & Sons)
- Stauffer, J. R., Schultz, G., & Kirkpatrick, J. D. 1998, *ApJ*, 499, 199
- Stello, D., & Nissen, P. E. 2001, *A&A*, 374, 105
- Strauss, M. A., et al. 1999, *ApJ*, 522, L61
- Testi, L, et al. 2001, *ApJ*, 552, L147
- Tsuji, T. 1986, *A&A*, 156, 8
- Tsuji, T. 1988, *A&A*, 197, 185
- Tsuji, T. 1991, *A&A*, 245, 203
- Tsuji, T. 2002, *ApJ*, 575, 264
- van Belle, G. T., et al. 1999, *AJ*, 117, 521
- Wallace, L., Meyer, M. R., Hinkle, K., & Edwards, S. 2000, *ApJ*, 535, 325
- Willing, B. A., Greene, T. P., & Meyer, M. R. 1999, *AJ*, 117, 469 (WGM99)
- Willing, B., Mikhail, A., Carlson, G., Meyer, M. R., & Greene, T. 2003, in *IAU Symp. 211, Brown Dwarfs*, ed. E. L. Martin (ASP), in press (astro-ph/0208264)
- Williams, D. M., Thompson, C. L., Rieke, G. H., & Montgomery, E. F. 1993, *SPIE*, 1946, 482
- Zapatero Osorio M. R., Béjar, V. J. S., Pavlenko, Ya., Rebolo, R., Allende Prieto, C., Martín, E. L., & García López, R. J. 2002a, *A&A*, 384, 937
- Zapatero Osorio, M. R., Béjar, V. J. S., Martín, E. L., Barrado y Navascués, D., & Rebolo, R. 2002b, *ApJ*, 569, L99

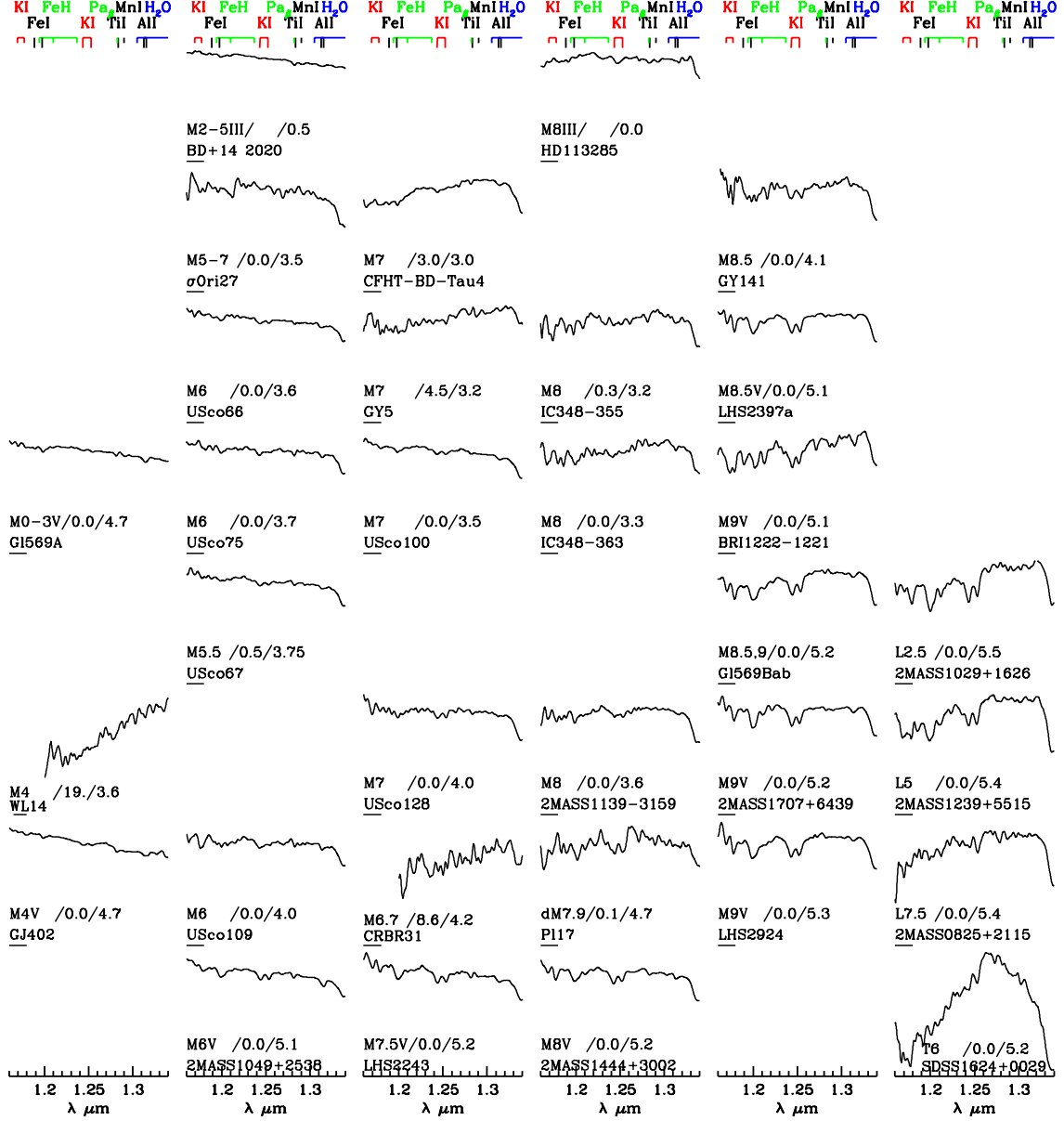


Fig. 1.— FSpec J-band spectra of program objects, arranged according to SpT in the horizontal direction and $\log(g)$ in the vertical. Zero-flux level is shown as a small dash below an object name. The abbreviation */*/* stands for SpT / A_V / $\log(g)$. Some of the lines identified on top may be absent in giants.

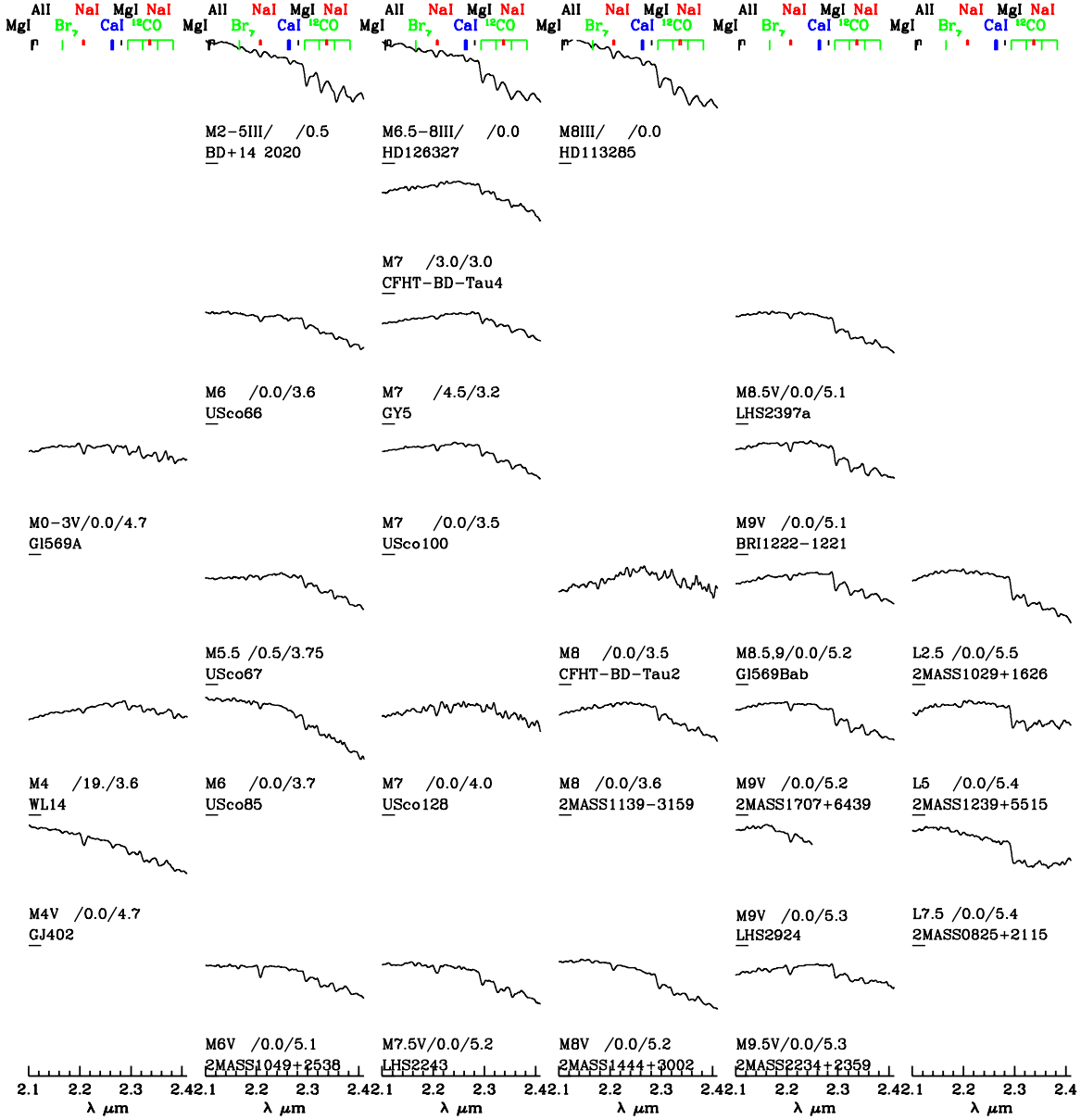


Fig. 2.— FSpec K band spectra. Same designations as in Fig. 1.

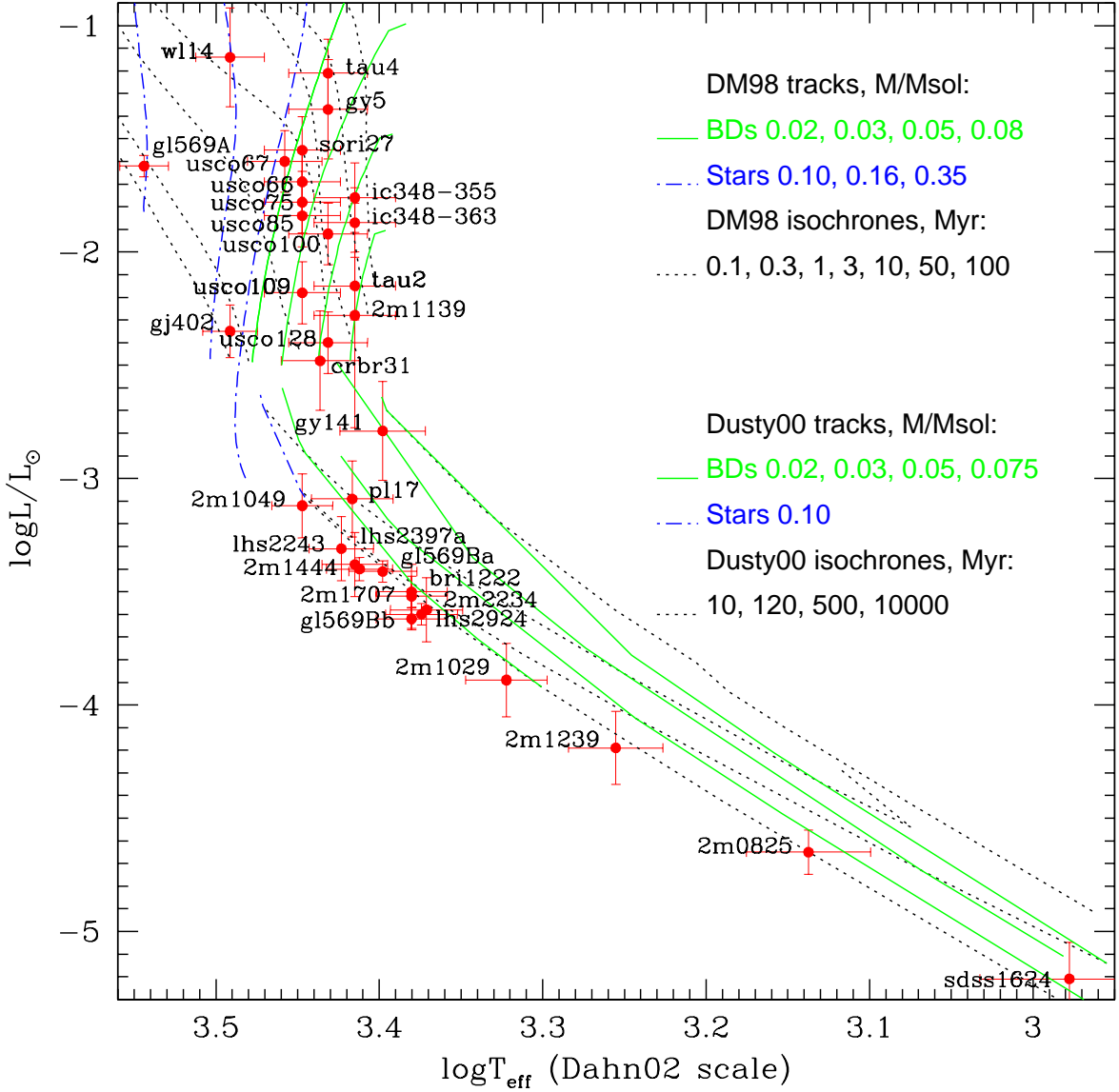


Fig. 3.— Program objects (except for giants), overlaid on D’Antona & Mazzitelli (1997, 1998) tracks (younger and more luminous objects) and on Chabrier et al. (2000) Dusty tracks. Temperature scale by Dahn et al. (2002) was used in this plot. Masses and ages are defined from right to left (towards increasing temperature). The figure is for guidance only to show relative positions of our targets on the H-R diagram (see § 3.1.4.)

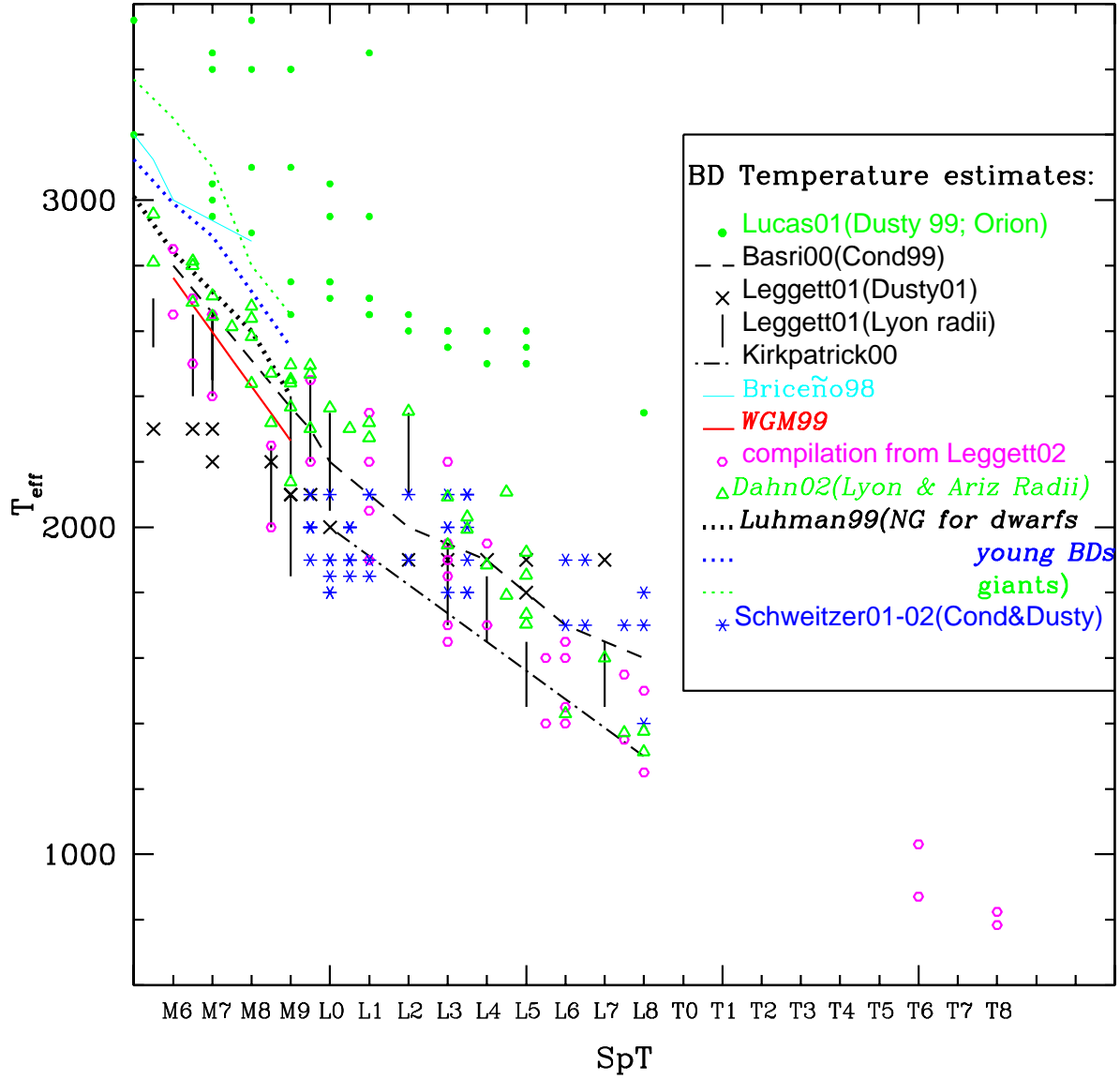


Fig. 4.— Some recent temperature scales drawn from the literature. Most of them were derived by comparison to model spectra by Lyon group (Cond and Dusty). The latest one, by Dahn et al. (2002) uses parallaxes and theoretical radii. In this work we considered three calibrations: by WGM99, Dahn02 and Luhman99.

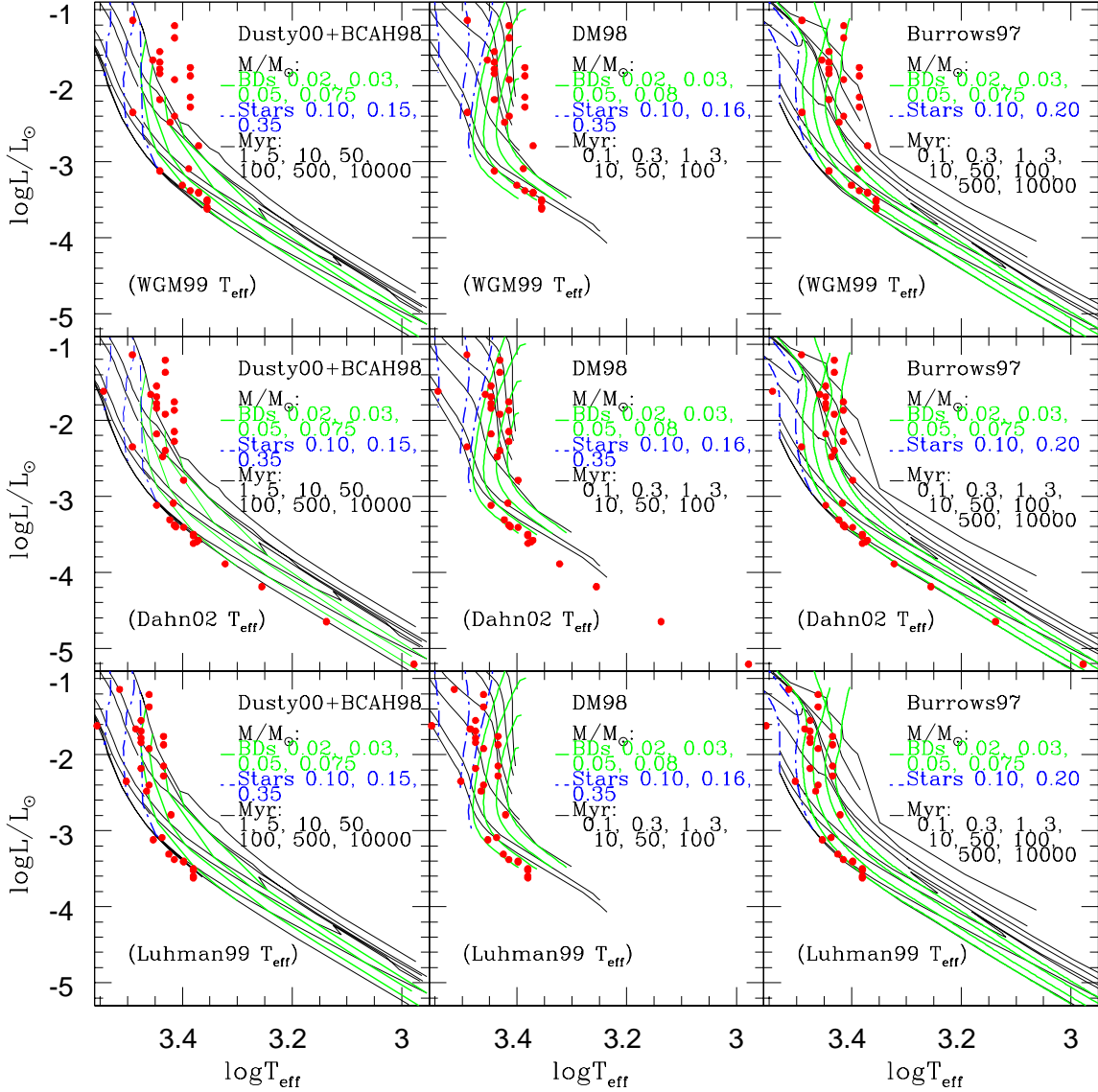


Fig. 5.— Program objects (dots) superimposed on the 3 sets of evolutionary tracks using 3 SpT– T_{eff} relations. Similar notation is used for tracks and isochrones as in Fig. 3. The figure shows how the choice of tracks and temperature scales influences derived masses and ages for low-mass objects.

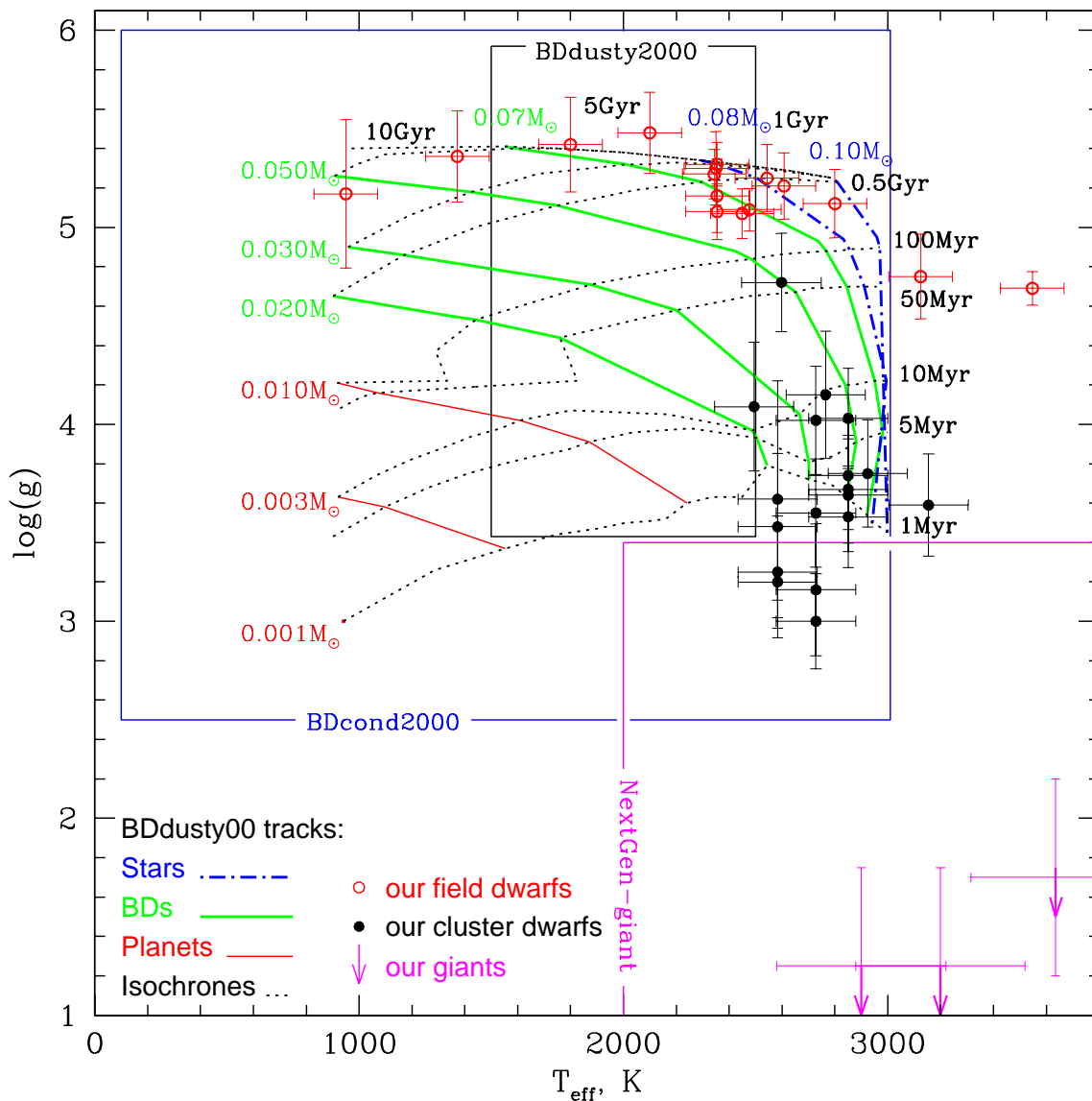


Fig. 6.— The *evolutionary models* of Chabrier et al. (2000) in terms of temperature and gravity. Members of young clusters are nicely separated by their gravities from older dwarfs and from giants of the same temperature. Also shown as rectangles are the boundaries of *synthetic spectra* grids by the PHOENIX group, which we used to compare to our dwarf spectra (BDdusty00 and BDcond00), and to giant HD113285 (NextGen-giant).

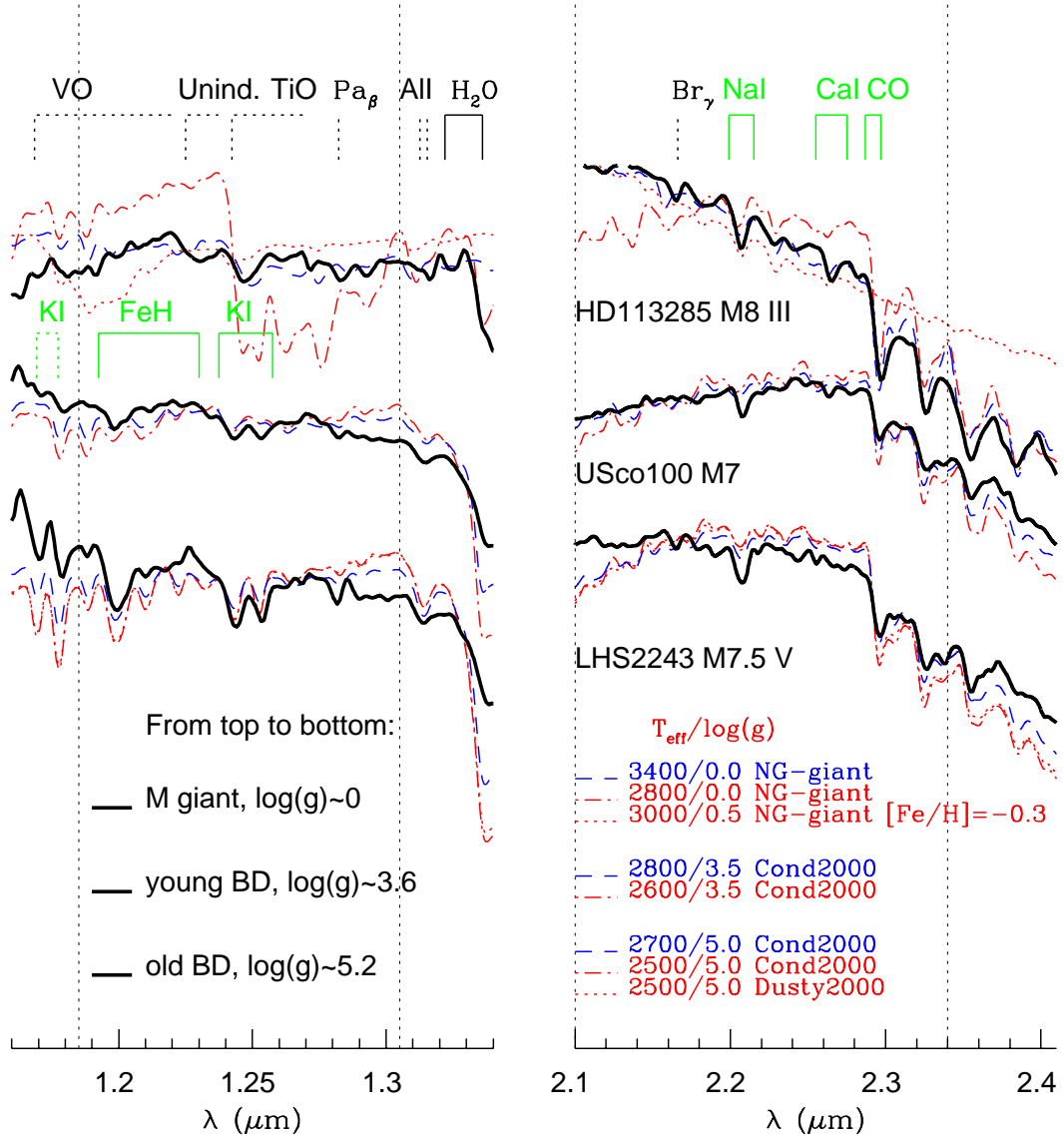


Fig. 7.— J and K spectra of a giant and two dwarfs of similar SpTs but different ages, overlaid on the theoretical spectra (of solar metallicity except where noted) with the expected range of temperatures and gravities. Solid lines define indices analyzed in this work for T_{eff} and gravity sensitivity, dotted – other prominent features including those relevant to giants only. K I, FeH & Na I lines are weaker in the younger, larger BD (USco100), as predicted by the models with lower gravity. H₂O is too strong while Na I line is too weak in models. Except for the H₂O band at 1.34 μm , the M giant spectrum is very distinctive with strong Na I, Ca I, CO and the presence of VO and TiO. Hydrogen lines and the edges of the spectral regions may contain some residuals from the telluric correction (§ 2.2). The spectra were normalized as described in § 2.2 – to have same integrated flux within the wavelength regions free from strong telluric water absorption (dotted vertical lines), and offset-ed by constant amount in the vertical direction for clarity.

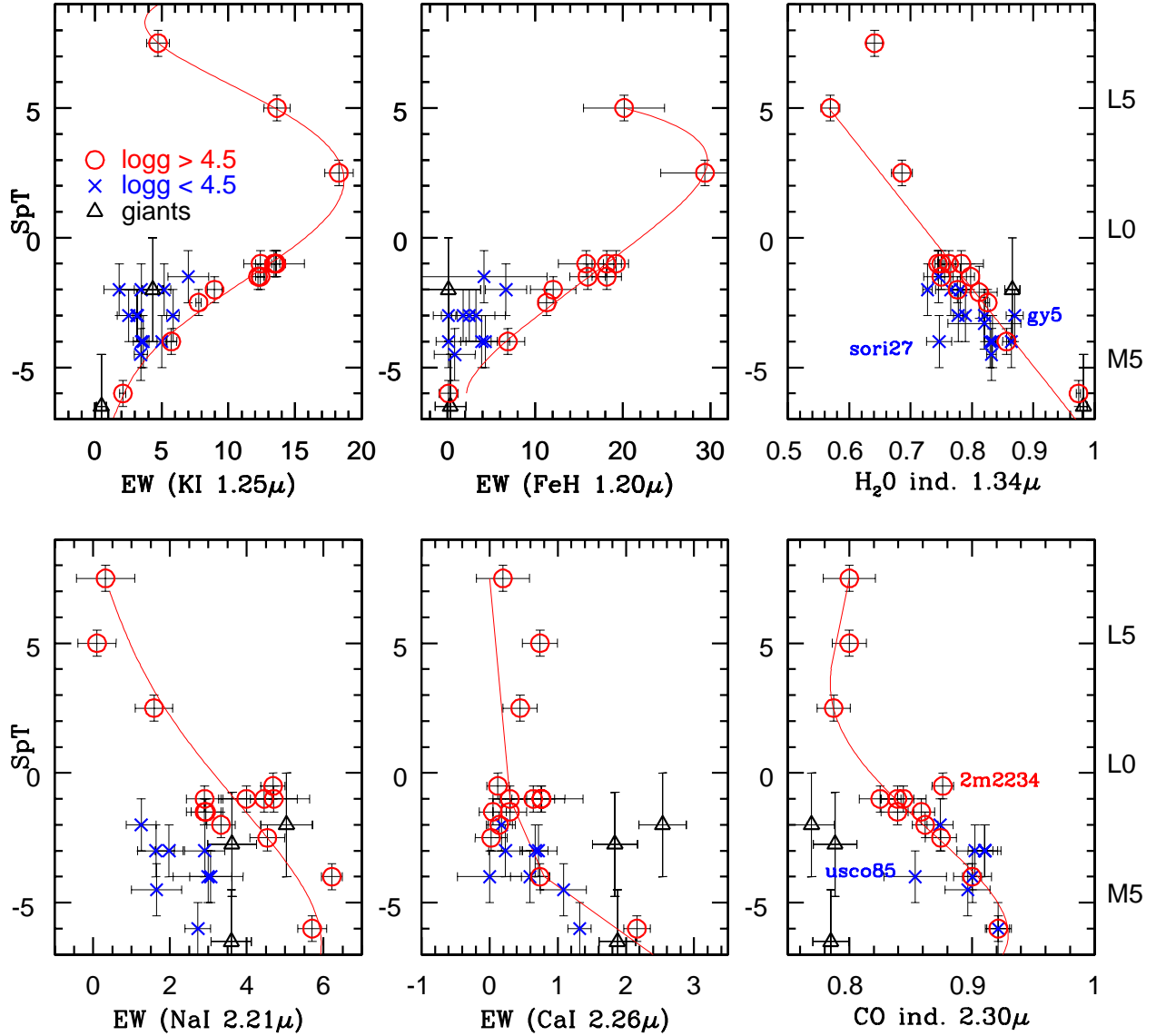


Fig. 8.— Plot of our index strength against SpT (M5 to L5). Field dwarfs and Pleiades member Pl 17 are represented by circles, cluster members by crosses, and giants by triangles. One can see that field objects always form an envelope, consistent with them having larger gravities and narrower gravity range. The scatter is relatively small for H₂O and CO indices. Giants occupy a distinctive place on these diagrams. The outliers are identified by name as they normally have lower S/N. Lines are drawn to represent schematically the behavior of the indices for dwarfs.

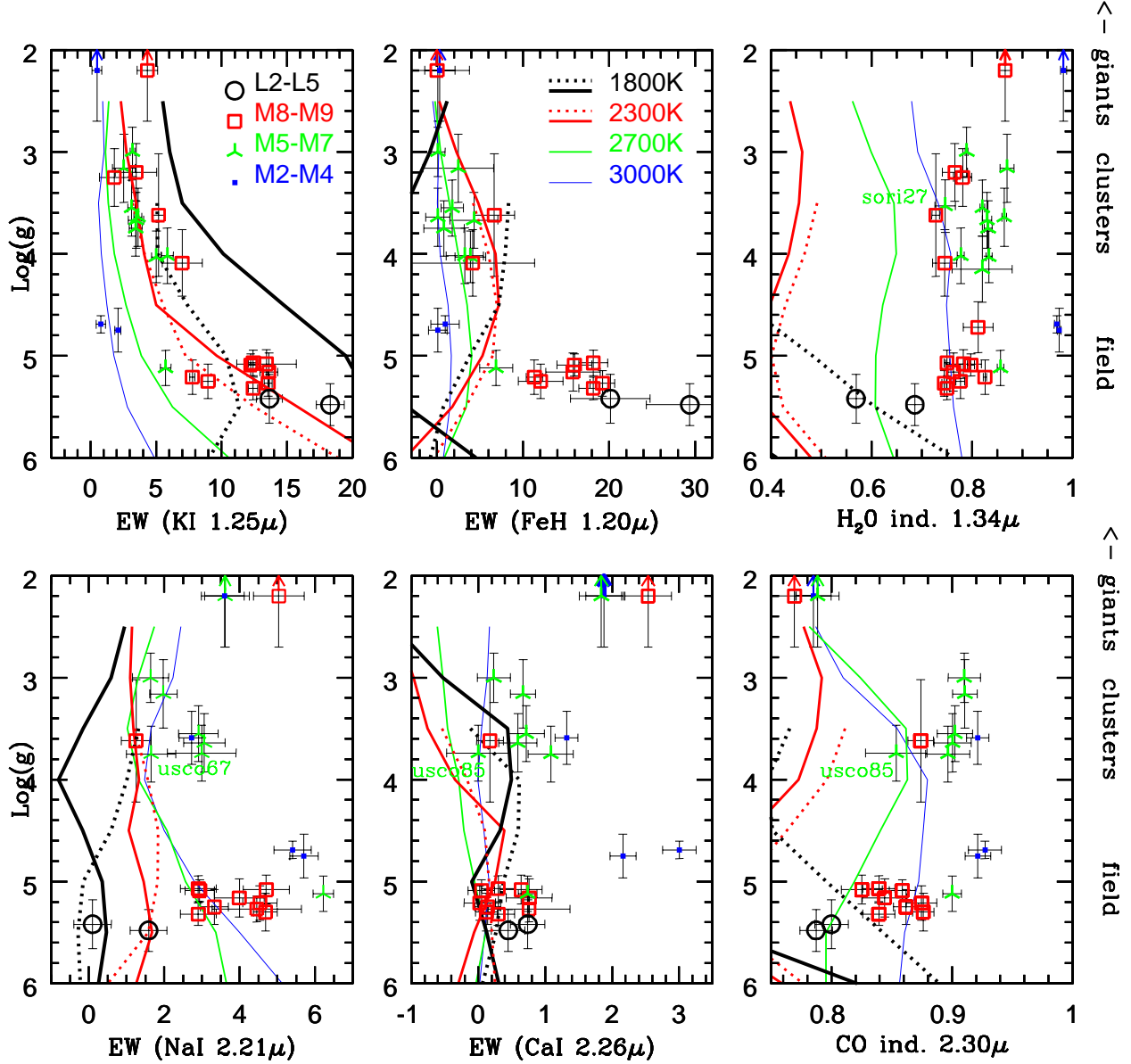


Fig. 9.— Plots of indices against $\log(g)$, as measured in program objects (symbols) and in models (dotted and dashed lines – BDdusty00, solid – BDcond00). Giants are represented by arrows as their gravities are out of range in this figure (~ 0 dex). Trends with T_{eff} and $\log(g)$ are clearly seen for all indices. The models generally predict correctly the qualitative behavior of features, but systematic offsets with observations persist.

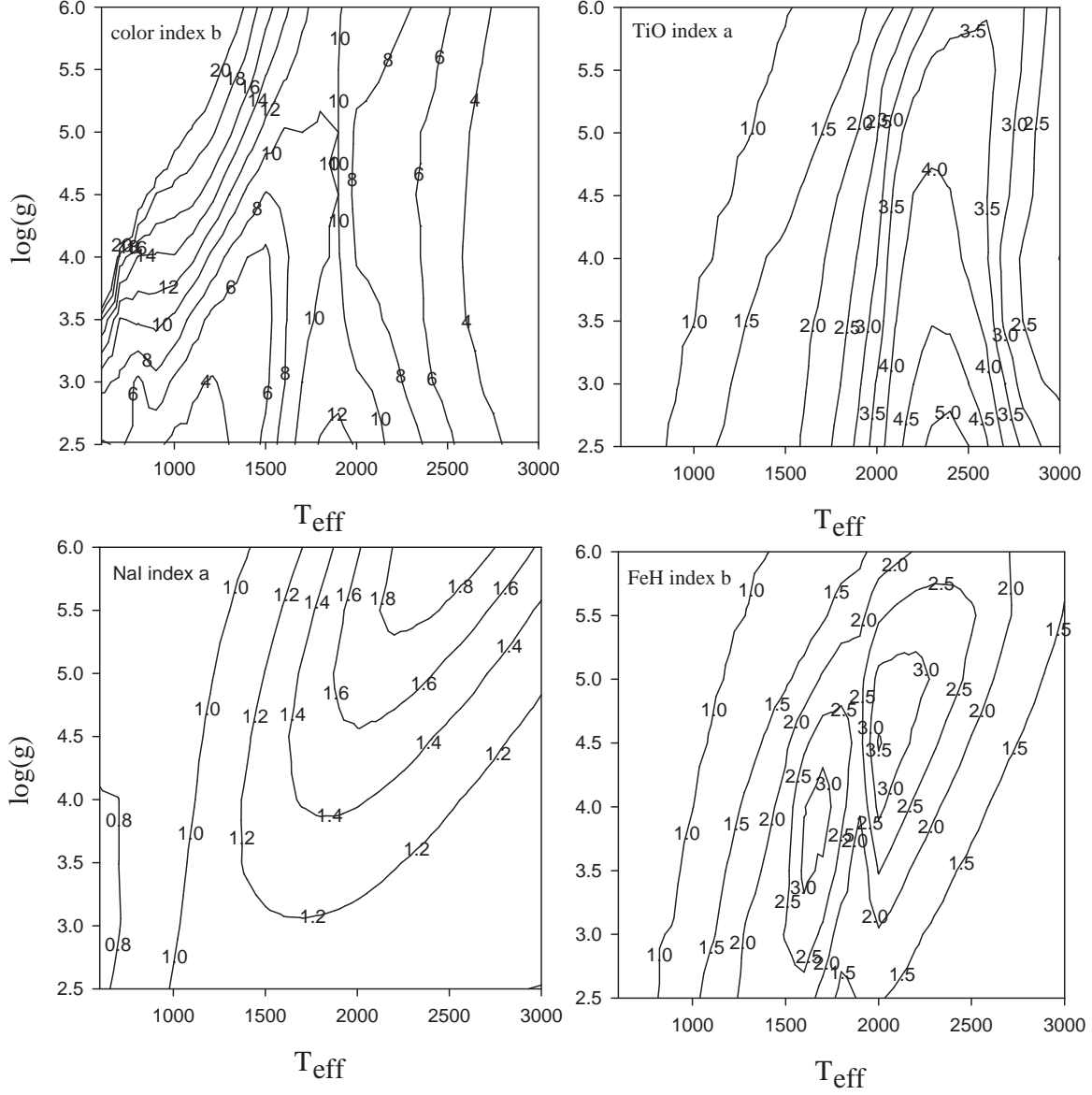


Fig. 10.— The representative contour plots of the indices used for spectral classification in the optical, as defined in Kirkpatrick et al. (1999). The indices were measured on BDcond00 model spectra, smoothed to the resolution of 9 \AA . The figure shows characteristic behavior of certain species, repeated also in the IR. One can see that the regions on $\log(g)$ – T_{eff} diagram where a given index would depend on only one parameter out of the two, are restricted. However, “color b” and “TiO a” indices are appropriate for most of the objects in our sample (where contours are nearly straight vertical lines).

Table 1. Program object properties taken from the literature

object name	SpT ^a	apparent mag	A_V	distance, pc	references ^b
<i>Cluster members:</i>					
IC348-355	M8 o	J = 14.65	0.3	318 ± 27	1,2,2,3
IC348-363	M8 o	J = 14.83	0.0	318 ± 27	2,2,2,3
CFHT-BD-Tau2	M8 o	J = 13.76	0.0	140 ± 10	4,4,4,5
CFHT-BD-Tau4	M7 o	J = 12.16	3.0	140 ± 10	4,4,4,5
SOri 27	M6 o	J = 14.86	0.0	473 ± 33	6,6,6,3
CRBR 31	M6.7 nir	J = 16.57	8.6	125 ± 25	7,8,7,3
GY 5 (CRBR 21)	M7 nir	J = 12.70	4.5	125 ± 25	10,8,10,3
GY 141	M8.5 o	J = 15.13	0.0	125 ± 25	11,8,11,3
WL 14 (CRBR 52, GY 172)	M4 nir	J = 16.12	19.2	125 ± 25	12,8,12,3
2MASSW J1139511-315921	M8 o	J = 12.67	0.0	73^{+25}_{-55}	13,13,,14
USco 66	M6 o	I = 14.85	0.0	145 ± 2	9,9,9,3
USco 67	M5.5 o	I = 14.87	0.5	145 ± 2	9,9,9,3
USco 75	M6 o	I = 15.08	0.0	145 ± 2	9,9,9,3
USco 85	M6 o	J = 13.03	0.0	145 ± 2	9,9,9,3
USco 100	M7 o	I = 15.62	0.0	145 ± 2	9,9,9,3
USco 109	M6 o	I = 16.06	0.0	145 ± 2	9,9,9,3
USco 128	M7 o	J = 14.41	0.0	145 ± 2	9,9,9,3
CFHT-P1 17	M7.9 o	J = 16.01	0.1	132 ± 15	15,15,15,16
<i>Field dwarfs:</i>					
GJ 402	M4e o	J = 7.30	0.0	5.6 ± 0.7	17,17,,18
Gl 569A	M0e/M3 ^c o	V = 10.14	0.0	9.8 ± 0.2	19/20,21,,18
Gl 569Ba	M8.5 nir	J = 11.14	0.0	9.8 ± 0.2	22,22,,18
Gl 569Bb	M9 nir	J = 11.65	0.0	9.8 ± 0.2	22,22,,18
BRI 1222-1221	M9 o	J = 12.56	0.0	17.1 ± 1	23,23,,24
LHS 2243	M7.5 o	J = 11.95	0.0	-	23,23,,
LHS 2397a ^d	M8.5 o	J = 11.93	0.0	14.3 ± 0.4	23,23,,35
LHS 2924	M9 o	J = 11.84	0.0	11.0 ± 0.2	17,17,,35
2MASSI J0825196+211552	L7.5 o	J = 15.12	0.0	10.7 ± 0.5	25,25,,24
2MASSI J1029216+162652	L2.5 o	J = 14.31	0.0	-	25,25,,
2MASSW J1049414+253852	M6 o	J = 12.40	0.0	-	23,23,,
2MASSW J1239272+551537 ^e	L5 o	J = 14.67	0.0	-	25,25,,

Table 1—Continued

object name	SpT ^a	apparent mag	A_V	distance, pc	references ^b
2MASSW J1444171+300214	M8 o	J = 11.68	0.0	-	23,23,,
2MASSW J1707183+643933	M9 o	J = 12.56	0.0	-	23,23,,
2MASSI J2234138+235956	M9.5 o	J = 13.14	0.0	-	23,23,,
SDSSp 162414.37+002915.6	T6 nir	J = 15.53	0.0	10.9 ± 0.3	26,27,,24
<i>Giants:</i>					
BD+14 2020	M2/M5 ^c III o	V = 10.1	-	-	28/29,30,,
HD 113285 (RT Vir)	M1/M8 ^f III o	J = 0.36 ± 1	0.0	138 ± 20	28/31,32,,18
HD 126327 (RX Boo)	M6.5e-M8e ^c III o	J = -0.59 ± 1	0.0	156 ± 24	31,33,34,18

^a“o” means optical SpT, “nir” – near-IR

^breferences given in the following order: reference for SpT, photometry, extinction, distance

^cmean SpT was adopted for T_{eff} estimation

^dM8/L7.5 binary with $\Delta J=3.83$ according to Freed, Close, & Siegler (2003)

^eL5/L5 binary according to Bouy et al. (2003)

^fIR colors favor M8, which was further adopted

References. — (1) Luhman et al. 1998; (2) Luhman 1999; (3) de Zeeuw et al. 1999; (4) Martín et al. 2001; (5) Kenyon, Dobrzycka, & Hartmann 1994; (6) Béjar et al. 2001; (7) Cushing, Tokunaga, & Kobayashi 2000; (8) Barsony et al. 1997; (9) Ardila, Martín, & Basri 2000; (10) Wilking, Greene, & Meyer 1999; (11) Luhman, Liebert, & Rieke 1997; (12) Luhman & Rieke 1999; (13) Gizis 2002; (14) Makarov & Fabricius 2001; (15) Martín et al. 2000; (16) Stello & Nissen 2001; (17) Leggett 1992; (18) The Hipparcos Catalog 1997; (19) The Third Catalog of Nearby Stars 1991; (20) Montes et al. 1997; (21) Hawley, Gizis, & Reid 1996; (22) Lane et al. 2001; (23) Gizis et al. 2000; (24) Dahn et al. 2002; (25) Kirkpatrick et al. 2000; (26) Geballe et al. 2002; (27) Strauss et al. 1999; (28) AGK3 Catalog 1975; (29) Jaschek, Conde & de Sierra 1964; (30) The Hipparcos and Tycho Catalogs 1997; (31) GCVS 1998; (32) Kerschbaum & Hron 1994; (33) Ducati 2002; (34) Perrin et al. 1998; (35) Monet et al. 1992.

Table 2. Observing log

object name	mag ^a	band	Yr-MM-DD	t_{exp} ^b	“S/N” ^c	Telluric Standard
<i>Cluster members:</i>						
IC348-355	14.7	J	2001-03-06	1920	44	HD 26710 G2V
IC348-363	14.8	J	2001-03-06	1920	62	HD 23169 G2V
CFHT-BD-Tau2	12.2	K	2002-03-26	1440	39	HD 27741 G0V
CFHT-BD-Tau4	12.2	J	2002-03-26	960	396	HD 27741 G0V
	10.3	K	2002-03-26	480	141	HD 27741 G0V
SOri 27	14.9	J	2001-03-06	1920	53	HD 160933 F9V
CRBR 31	16.6	J	2001-05-06	2880	18	HD 146997 G2V
GY 5	12.7	J	2002-03-27	1320	80	HD 147284 G3V
	10.9	K	2002-03-29	960	185	HD 147284 G3V
GY 141	15.1	J	2001-05-07	2880	46	HD 146997 G2V
WL 14	16.1	J	2001-05-07	2880	18	HD 146997 G2V
	11.7	K	2001-05-07	960	205	HD 146997 G2V
2MASSW J1139511-315921	12.7	J	2002-03-29	960	141	HD 100585 G3V
	11.5	K	2002-03-26	480	176	HD 100585 G3V
USco 66	≈ 12.7	J	2002-03-27	1920	233	HD 141092 G3V
	≈ 12.0	K	2002-03-27	960	123	HD 141092 G3V
USco 67	≈ 12.7	J	2002-03-29	2400	142	HD 142523 G1/G2V
	≈ 11.8	K	2002-03-29	960	104	HD 142523 G1/G2V
USco 75	≈ 12.9	J	2001-05-06	960	118	HD 146997 G2V
USco 85	≈ 12.1	K	2002-03-28	960	75	HD 142523 G1/G2V
USco 100	≈ 13.2	J	2002-03-27	1440	253	HD 141092 G3V
	≈ 12.2	K	2002-03-27	960	130	HD 141092 G3V
USco 109	≈ 13.9	J	2001-05-06	960	185	HD 146997 G2V
USco 128	14.4	J	2002-03-27	2400	152	HD 142523 G1/G2V
	≈ 13.5	K	2002-03-29	1440	47	HD 142523 G1/G2V
CFHT-P1 17	16.0	J	2001-03-06	3840	37	HD 23169 G2V
<i>Field dwarfs:</i>						
GJ 402	7.3	J	2002-03-28	160	303	HD 88725 G1V
	6.4	K	2002-03-28	160	180	HD 88725 G1V
Gl 569A	≈ 7.0	J	2001-03-04	20	202	HD 131473 F9V
	≈ 6.2	K	2001-03-04	260	139	HD 131473 F9V

Table 2—Continued

object name	mag ^a	band	Yr-MM-DD	t _{exp} ^b	“S/N” ^c	Telluric Standard
Gl 569Bab ^d	10.6	J	2001-03-04	960	199	HD 131473 F9V
	9.5	K	2001-03-04	260	142	HD 131473 F9V
BRI 1222-1221	12.6	J	2001-03-05	480	31	HD 108799 G1/G2V
	11.4	K	2001-03-05	240	111	HD 108799 G1/G2V
LHS 2243	12.0	J	2002-03-26	1440	351	HD 91950 G2V
	11.0	K	2002-03-26	480	150	HD 91950 G2V
LHS 2397a	11.9	J	2002-03-27	960	164	HD 98298 G3V
	10.7	K	2002-03-27	480	176	HD 98298 G3V
LHS 2924	11.8	J	2001-03-05	480	228	HD 134044 F8V
	10.7	K	2001-03-05	480	57	HD 134044 F8V
2MASSI J0825196+211552	15.1	J	2001-05-06	2880	83	HD 68255 F9V
	13.1	K	2001-05-07	1440	90	HD 68257 F7V
2MASSI J1029216+162652	14.3	J	2001-05-06	960	66	HD 87776 G0V
	12.6	K	2001-05-06	960	140	HD 87776 G0V
2MASSW J1049414+253852	12.4	J	2002-03-26	960	173	HD 91950 G2V
	11.4	K	2002-03-26	960	250	HD 91950 G2V
2MASSW J1239272+551537	14.7	J	2001-05-07	1920	71	HD 108954 F9V
	12.7	K	2001-05-08	2400	137	HD 108954 F9V
2MASSW J1444171+300214	11.7	J	2001-03-05	480	127	HD 129357 G2V
	10.6	K	2001-03-05	240	183	HD 129357 G2V
2MASSW J1707183+643933	12.6	J	2001-03-05	480	105	HD 160933 F9V
	11.4	K	2001-03-05	240	103	HD 160933 F9V
2MASSI J2234138+235956	11.8	K	2001-05-07	960	216	HD 210211 G2V
SDSSp 162414.37+002915.6	15.5	J	2001-05-08	2880	21	HD 140538 G2.5V
<i>Giants:</i>						
BD+14 2020	$\approx 6 \pm 1$	J	2002-03-27	160	188	HD 75528 G1V
	$\approx 5 \pm 1$	K	2002-03-27	160	130	HD 75528 G1V
HD 113285	0.4 ± 1	J	2002-03-27	20	89	HD 114606 G1V
	-1.1 ± 1	K	2002-03-28	30	101	HD 114606 G1V
HD 126327	-2.0 ± 1	K	2002-03-28	100	107	HD 126991 G2V

^a“ \approx ” means that the given magnitude was estimated from other magnitudes, which are reported in Table 1

^btotal exposure time in seconds

^c“S/N” is the ratio of the average flux and dispersion between 1.29–1.31 and 2.22–2.26 μm measured on the final, smoothed spectra. This is a good measurement of the relative quality of spectra, see § 4.1 for details

^dcomposite spectrum

Table 3. Program object properties derived in this work

object name	$(M_J)_0$	$\log(L/L_\odot)$	T_{eff}^a	M/M_\odot^a	$\log(g)^a$
<i>Cluster members:</i>					
IC348-355	7.06	-1.76 ± 0.15	2583 ± 150	0.028 ± 0.015	3.20 ± 0.28
IC348-363	7.32	-1.87 ± 0.15	2583 ± 150	0.026 ± 0.015	3.25 ± 0.28
CFHT-BD-Tau2	8.03	-2.15 ± 0.15	2583 ± 150	0.022 ± 0.015	3.48 ± 0.37
CFHT-BD-Tau4	5.63	-1.21 ± 0.15	2729 ± 150	0.058 ± 0.030	3.00 ± 0.24
SOri 27	6.48	-1.55 ± 0.15	2851 ± 150	0.069 ± 0.035	3.53 ± 0.26
CRBR 31	8.81	-2.48 ± 0.22	2765 ± 150	0.041 ± 0.015	4.15 ± 0.32
GY 5	6.02	-1.37 ± 0.22	2729 ± 150	0.056 ± 0.035	3.16 ± 0.34
GY 141	9.64	-2.79 ± 0.22	2494 ± 150	0.024 ± 0.015	4.09 ± 0.33
WL 14	5.54	-1.14 ± 0.22	3155 ± 150	0.144 ± 0.040	3.59 ± 0.26
2MASSW J1139511-315921	8.35	-2.28 ± 0.50	2583 ± 150	0.022 ± 0.015	3.62 ± 0.60
USco 66	6.84	-1.69 ± 0.14	2851 ± 150	0.066 ± 0.035	3.64 ± 0.29
USco 67	6.61	-1.60 ± 0.14	2924 ± 150	0.081 ± 0.040	3.75 ± 0.27
USco 75	7.07	-1.78 ± 0.14	2851 ± 150	0.059 ± 0.030	3.67 ± 0.27
USco 85	7.22	-1.84 ± 0.14	2851 ± 150	0.058 ± 0.030	3.74 ± 0.27
USco 100	7.41	-1.92 ± 0.14	2672 ± 150	0.041 ± 0.020	3.55 ± 0.27
USco 109	8.05	-2.18 ± 0.14	2851 ± 150	0.054 ± 0.020	4.03 ± 0.25
USco 128	8.60	-2.40 ± 0.14	2729 ± 150	0.039 ± 0.015	4.02 ± 0.27
CFHT-P1 17	10.36	-3.09 ± 0.17	2598 ± 150	0.047 ± 0.025	4.72 ± 0.25
<i>Field dwarfs:</i>					
GJ 402	8.56	-2.35 ± 0.12	3125 ± 120	0.121 ± 0.050	4.75 ± 0.22
Gl 569A	7.04	-1.62 ± 0.05	3548 ± 120	0.350 ± 0.030	4.69 ± 0.09
Gl 569Ba	11.18	-3.41 ± 0.05	2449 ± 120	0.059 ± 0.015	5.07 ± 0.13
Gl 569Bb	11.69	-3.62 ± 0.05	2355 ± 120	0.075 ± 0.010	5.32 ± 0.12
BRI 1222-1221	11.39	-3.50 ± 0.07	2355 ± 120	0.057 ± 0.015	5.08 ± 0.14
LHS 2243	10.94 ^b	-3.31 ± 0.14	2608 ± 120	0.073 ± 0.010	5.21 ± 0.17
LHS 2397a	11.15	-3.40 ± 0.05	2477 ± 120	0.061 ± 0.010	5.09 ± 0.11
LHS 2924	11.63	-3.60 ± 0.05	2344 ± 120	0.071 ± 0.015	5.27 ± 0.11
2MASSI J0825196+211552	14.97	-4.65 ± 0.10	1372 ± 120	0.065 ± 0.020	5.36 ± 0.23
2MASSI J1029216+162652	12.64 ^b	-3.89 ± 0.16	2100 ± 120	0.068 ± 0.015	5.48 ± 0.21
2MASSW J1049414+253852	10.43 ^b	-3.12 ± 0.14	2801 ± 120	0.075 ± 0.015	5.12 ± 0.17
2MASSW J1239272+551537	13.50 ^b	-4.19 ± 0.16	1800 ± 120	0.075 ± 0.025	5.42 ± 0.24

Table 3—Continued

object name	$(M_J)_0$	$\log(L/L_\odot)$	T_{eff}^a	M/M_\odot^a	$\log(g)^a$
2MASSW J1444171+300214	11.11 ^b	-3.38 ± 0.14	2543 ± 120	0.076 ± 0.010	5.25 ± 0.17
2MASSW J1707183+643933	11.45 ^b	-3.52 ± 0.14	2355 ± 120	0.062 ± 0.015	5.16 ± 0.19
2MASSI J2234138+235956	11.62 ^b	-3.58 ± 0.14	2350 ± 120	0.073 ± 0.015	5.30 ± 0.19
SDSSp 162414.37+002915.6	15.34	$-5.21^c \pm 0.16$	950 ± 120	0.048 ± 0.030	5.17 ± 0.38
<i>Averages</i>					
for cluster	7.51 ± 1.31	-1.95 ± 0.52	2743 ± 163	0.052 ± 0.029	3.68 ± 0.42
for field	11.54 ± 2.04	-3.52 ± 0.82	2345 ± 613	0.088 ± 0.071	5.17 ± 0.21
<i>Giants:</i>					
BD +14 2020	-	-	3635 ± 320	1–5	0.5 ± 0.5
HD 113285	-5.34	3.30 ± 0.42	2900 ± 320	1–5	0.0 ± 0.5
HD 126327	-6.56	3.78 ± 0.40	3200 ± 320^d	1–5	0.0 ± 0.5

^aMean values from 3 temperature scales and 3 sets of tracks (§ 3.1.4). Error estimates are described in § 3.1.5

^bDerived from M_J -SpT relationship for field dwarfs from Dahn et al. (2002)

^cLuminosity adopted equal to that of Gl229B

^dPerrin et al. (1998) measured 2786 ± 46 K for this star

Table 4. Definition of indices considered in this work (μm)

name	PC1	PC2	F1	F2	PC3	PC4
FeH	1.1890	1.1960	1.1925	1.2300	1.2265	1.2335
K I	1.2340	1.2410	1.2375	1.2575	1.2540	1.2610
H ₂ O	1.3340	1.3380			1.3200	1.3240
Na I	2.1950	2.2030	2.1990	2.2150	2.2110	2.2190
Ca I	2.2525	2.2575	2.2625	2.2675	2.2725	2.2775
CO	2.2960	2.2980			2.2860	2.2880

Note. — H₂O and CO indices have been defined as the ratio of fluxes averaged between pseudo-continuum regions PC1-PC2 and PC3-PC4. Larger value of flux ratio corresponds to weaker absorption feature. Rest indices measure equivalent width of absorption lines. PC1-PC2 and PC3-PC4 define continuum level while F1 and F2 define the wavelength interval for EW integration.

Table 5. Measurements of indices defined in Table 4

object name	EW(K I), Å	EW(FeH), Å	H ₂ O ind	EW(Na I), Å	EW(Ca I), Å	CO ind
<i>Cluster members:</i>						
IC348-355	3.48 ± 1.58	-	0.766 ± 0.025	-	-	-
IC348-363	1.82 ± 1.13	-	0.781 ± 0.018	-	-	-
CFHT-BD-Tau2	-	-	-	-	-	-
CFHT-BD-Tau4	3.19 ± 0.18	0 ± 0.83	0.789 ± 0.003	1.63 ± 0.48	0.23 ± 0.25	0.910 ± 0.013
SOri 27	-	-	0.747 ± 0.020	-	-	-
CRBR 31	-	-	0.820 ± 0.059	-	-	-
GY 5	2.54 ± 0.87	2.47 ± 4.13	0.869 ± 0.014	1.98 ± 0.37	0.67 ± 0.19	0.911 ± 0.010
GY 141	6.99 ± 1.52	4.15 ± 7.18	0.746 ± 0.024	-	-	-
WL 14	-	-	-	2.73 ± 0.33	1.32 ± 0.17	0.921 ± 0.009
2MASSW J1139511-315921	5.19 ± 0.49	6.66 ± 2.33	0.728 ± 0.008	1.25 ± 0.38	0.18 ± 0.20	0.874 ± 0.011
USco 66	3.62 ± 0.30	0 ± 1.41	0.864 ± 0.005	3.07 ± 0.55	0.59 ± 0.28	0.900 ± 0.015
USco 67	3.44 ± 0.49	0.82 ± 2.33	0.832 ± 0.008	1.65 ± 0.65	1.08 ± 0.34	0.896 ± 0.018
USco 75	3.48 ± 0.59	4.29 ± 2.79	0.830 ± 0.009	-	-	-
USco 85	-	-	-	2.99 ± 0.91	0.00 ± 0.47	0.854 ± 0.025
USco 100	3.14 ± 0.28	1.76 ± 1.30	0.820 ± 0.004	2.91 ± 0.52	0.72 ± 0.27	0.902 ± 0.015
USco 109	5.02 ± 0.38	3.90 ± 1.78	0.834 ± 0.006	-	-	-
USco 128	5.85 ± 0.46	3.23 ± 2.17	0.777 ± 0.007	-	-	-
CFHT-P1 17	-	-	0.812 ± 0.030	-	-	-
<i>Field dwarfs:</i>						
GJ 402	2.10 ± 0.23	0 ± 1.09	0.974 ± 0.004	5.71 ± 0.38	2.16 ± 0.19	0.921 ± 0.010
G1 569A	0.78 ± 0.34	0.94 ± 1.63	0.969 ± 0.005	5.41 ± 0.49	3.00 ± 0.25	0.927 ± 0.014
G1 569Bab	12.41 ± 0.35	18.15 ± 1.66	0.750 ± 0.005	2.90 ± 0.48	0.30 ± 0.25	0.839 ± 0.013
BRI 1222-1221	13.42 ± 2.28	-	0.783 ± 0.036	4.71 ± 0.61	0.64 ± 0.31	0.825 ± 0.017

Table 5—Continued

object name	EW(K I), Å	EW(FeH), Å	H ₂ O ind	EW(Na I), Å	EW(Ca I), Å	CO ind
LHS 2243	7.77 ± 0.20	11.30 ± 0.94	0.826 ± 0.003	4.54 ± 0.45	$0.02 \text{ } 0.23$	0.875 ± 0.013
LHS 2397a	12.22 ± 0.43	15.96 ± 2.01	0.798 ± 0.007	2.94 ± 0.38	0.05 ± 0.20	0.859 ± 0.011
LHS 2924	13.55 ± 0.31	19.20 ± 1.45	0.745 ± 0.005	4.46 ± 1.19	0.76 ± 0.61	-
2MASSI J0825196+211552	4.73 ± 0.84	-	0.641 ± 0.013	0.32 ± 0.75	0.20 ± 0.39	0.800 ± 0.021
2MASSI J1029216+162652	18.28 ± 1.07	29.35 ± 5.03	0.686 ± 0.017	1.58 ± 0.48	0.45 ± 0.25	0.787 ± 0.013
2MASSW J1049414+253852	5.73 ± 0.40	6.87 ± 1.91	0.856 ± 0.006	6.22 ± 0.27	0.74 ± 0.14	0.900 ± 0.008
2MASSW J1239272+551537	13.65 ± 0.98	20.13 ± 4.62	0.569 ± 0.015	0 ± 0.50	0.74 ± 0.25	0.800 ± 0.014
2MASSW J1444171+300214	8.97 ± 0.55	12.03 ± 2.59	0.777 ± 0.009	3.33 ± 0.37	0.14 ± 0.19	0.862 ± 0.010
2MASSW J1707183+643933	13.61 ± 0.67	15.80 ± 3.15	0.763 ± 0.010	3.99 ± 0.66	0.76 ± 0.34	0.844 ± 0.018
2MASSI J2234138+235956	-	-	-	4.69 ± 0.31	0.12 ± 0.16	0.876 ± 0.009
SDSSp 162414.37+002915.6	7.68 ± 3.33	6.98 ± 15.7	0.118 ± 0.052	-	-	-
<i>Giants:</i>						
BD +14 2020	0.49 ± 0.37	0.32 ± 1.75	0.982 ± 0.006	3.60 ± 0.52	1.88 ± 0.27	0.785 ± 0.015
HD 113285	4.33 ± 0.78	0 ± 3.69	0.866 ± 0.012	5.04 ± 1.06	2.54 ± 0.54	0.769 ± 0.029
HD 126327	-	-	-	3.62 ± 0.64	1.84 ± 0.33	0.789 ± 0.018

Note. — “0” indicates where measured EW was negative but small; “-” indicates that either feature was completely buried in the noise or that we did not have J or K spectrum.

Errors described in §4.1